Joint measurements of complementary properties of quantum systems

By

Guillaume Thekkadath

A thesis completed under the supervision of J. S. Lundeen
submitted to the Faculty of Graduate and Postgraduate studies
in partial fulfillment of the requirements for the for the degree of

Masters of Science

in Physics

Department of Physics
University of Ottawa

Abstract

In quantum mechanics, measurements disturb the state of the system being measured. This disturbance is largest for complementary properties (*e.g.* position and momentum) and hence limits the precision with which such properties can be determined simultaneously. Often, this fact is conflated with Heisenberg's uncertainty principle, which refers to an uncertainty relation between complementary properties that is intrinsic to quantum states. In this thesis, the distinction between these two fundamental characteristics of quantum mechanics is made clear. At the intersection of the two are "joint measurements", which circumvent measurement disturbance to simultaneously determine complementary properties. They have applications in quantum metrology and enable a direct measurement of quantum states. The focus of this thesis is on the latter.

The thesis is structured in the following way. The first chapter serves as an introduction to joint measurements. It surveys the seminal works in the field, doing so in a chronological manner to provide some historical context. The remainder of the thesis discusses two strategies to experimentally achieve joint measurements. The first strategy is to sequentially measure the complementary properties, making these measurements weak so that they do not disrupt each other. The second strategy is to first clone the system being measured, and then measure each complementary property on a separate clone. Both strategies are experimentally demonstrated on polarized photons, but can be readily extended to other systems.

Résumé

En mécanique quantique, l'état d'un système est perturbé lorsqu'on le mesure, surtout si l'on mesure ses propriétés complémentaires (p. ex. position et impulsion). Cette perturbation limite la précision d'une mesure simultanée de propriétés complémentaires. Il est important de comprendre que cette limite est induite par la mesure, et qu'elle n'est donc pas une conséquence du principe d'incertitude de Heisenberg, qui est plutôt une limite inhérente aux états quantiques. D'une part, cette thèse clarifie la distinction entre ces deux caractéristiques fondamentales de la mécanique quantique. D'autre part, elle présente également les « mesures conjointes ». Celles-ci contournent la perturbation d'une mesure pour déterminer simultanément des propriétés complémentaires. Les mesures conjointes sont utiles en métrologie quantique et permettent une mesure directe des états quantiques. Cette thèse se concentre sur ce dernier point.

La thèse est structurée de la manière suivante. Le premier chapitre est une introduction aux mesures conjointes. Il propose une vue d'ensemble sur les travaux fondateurs, de manière chronologique, de façon à fournir un contexte historique. Par la suite, la thèse présente deux stratégies visant à réaliser des mesures conjointes en laboratoire. La première stratégie consiste à mesurer séquentiellement les propriétés complémentaires. Les mesures sont délibérément faibles pour éviter qu'elles ne se perturbent entre elles. La deuxième stratégie consiste à d'abord cloner le système, et ensuite à mesurer chaque propriété complémentaire sur un clone séparé. Les deux stratégies, qui sont démontrées avec des photons polarisés, peuvent être aussi utilisées avec d'autres systèmes.

Acknowledgements

I acknowledge the generous financial support from the Natural Sciences and Engineering Research Council of Canada and the University of Ottawa.

I am indebted to my supervisor, Jeff Lundeen, for his continued guidance and an endless supply of fascinating projects. His unassuming approach to research and science is a source of inspiration. This approach is reflected by his simple but clear writing style, which is something I hope to carry forward throughout my career.

I gratefully recognize the help of the Lundeen lab post-doc, Lambert Giner, whose Labview codes automated my experiments. In fact, computers did most of the work in this thesis (they never get their due credit). I also had the pleasure of working with Rebecca Saaltink, who graciously showed me the ropes of her cloning apparatus.

I am fortunate to have been a part of the CERC group. Thank you for the fun squash matches Kashif and Shayan, and thank you to my officemates for the lively physics conversations (especially Akbar, who always asked difficult yet simple questions).

It is important to strike a balance with life outside the dark depths of the lab. As such, I cannot stress enough the importance of my weekly retreat to HoolNation with friends.

Most importantly, I am grateful for my family's unconditional, unequivocal, and loving support.

List of publications

The following papers were published/submitted during the completion of my masters (in chronological order). Not all pertain to the subject of this thesis.

1. G. S. Thekkadath, L. Jiang, J. H. Thywissen, “Spin correlations and entanglement in partially magnetised ensembles of fermions", *J. Phys. B: At. Mol. Opt. Phys.* **49** 21 (2016).

2. G. S. Thekkadath, K. Heshami, D. G. England, P. J. Bustard, B. J. Sussman, M. Spanner, “Optical quantum memory for ultrafast photons using molecular alignment", *J. Mod. Opt.* **63** 20 (2016).

3. G. S. Thekkadath, L. Giner, Y. Chalich, M. J. Horton, J. Banker, J. S. Lundeen, “Direct measurement of the density matrix of a quantum system", *Phys. Rev. Lett.* **117** 120401 (2016).

4. G. S. Thekkadath, R. Y. Saaltink, L. Giner, J. S. Lundeen, “Determining complementary properties with quantum clones", *Phys. Rev. Lett.* **119** 050405 (2017).

5. K. T. Kaczmarek, P. M. Ledingham, B. Brecht, S. E. Thomas, G. S. Thekkadath, O. Lazo-Arjona, J. H. D. Munns, E. Poem, A. Feizpour, D. J. Saunders, J. Nunn, I. A. Walmsley, “A room-temperature noise-free quantum memory for broadband light”, arXiv:1704.00013 (2017).

Author contributions

The work presented in this thesis is the product of scientific collaboration. Here I give a detailed account of my specific contributions to each project.

The first project (Ch. 3) is the direct measurement of the density matrix experiment. The idea was initially proposed by J. Lundeen and C. Bamber in Ref. [54]. The experimental setup was designed by co-authors, except for the mixed state generation procedure, which I proposed and built. The experimental apparatus was already built by co-authors upon my arrival. However, the experiment was not functioning as expected due to poor alignment and technical noise. To this end, I developed a procedure for aligning the walk-off crystals. Furthermore, I wrote code to post-process (e.g. Fourier filter) and analyze the data. These steps were critical for the progression of the project. I performed the final data collection. Finally, I wrote the initial draft of the paper, which was then edited by J. Lundeen and myself. Other co-authors also contributed minor edits.

The second project (Ch. 5) is the cloning experiment. The idea was proposed theoretically by H. Hofmann in Ref. [38]. J. Lundeen proposed a rough outline for an experimental setup to implement the idea with polarization qubits, which was further refined with the help of L. Giner and R. Saaltink. The photon source and interferometer were built upon my arrival, but many issues prevented further progress. I contributed to debugging the experimental setup in order to get it functioning optimally. At that point, I proposed a method to transition from optimal to trivial cloning, and supplied my mixed state generator used in the previous experiment. I then wrote code to process the final data, which I collected myself. Finally, I wrote the initial draft of the paper, which was then edited by J. Lundeen and myself. Other co-authors also contributed minor edits.

As soon as we watch atoms they behave differently.
Cartoon drawn by P. Evers and taken from Ref. [49].

Contents

Chapter 1

Overview of joint measurements from historical perspective

In this chapter, I provide a broad overview of the topic of joint measurements in quantum mechanics from a historical perspective. To the best of my knowledge, there is no comprehensive review on this topic. This is partly because joint measurement have only recently been experimentally accessible, as will be made evident below. I do my best to survey some of the seminal works on the subject.

Figure 1.1: "*The more precisely position is determined, the more imprecisely momentum will be known, and vice versa.*"-W. Heisenberg, translated from Ref. [37]. Figure taken from Ref. [34].

1.1 Heisenberg uncertainty principle and measurement disturbance

The history of joint measurements begins with the inception of quantum mechanics. Two formalisms emerged in the 1920s that aimed to close the theoretical gaps in our description of the microscopic world, notably the discreteness of atomic spectra and the ultraviolet catastrophe. The first formalism was the matrix mechanics of Heisenberg, Born, and Jordan, while the second was Schrödinger's wave mechanics. Both were built upon the essential contributions of the early figures in the history of quantum physics, such as Einstein, Planck, and de Broglie. Although the two formalisms are mathematically equivalent, each provides a different perspective that is essential to understand joint measurements.

Matrix mechanics uses the mathematical ideas of Hilbert to describe quantum systems as algebraic objects. The state of a general quantum system is described by a vector, *e.g.* $|\Psi\rangle$, that contains all the information about the system's physical properties. This vector lives in a Hilbert space, $|\Psi\rangle \in \mathscr{H}$, which is an algebraical space encompassing every possible state that a particular physical system could have. Moreover, $\mathscr{H}$ is also home to matrices that describe transformations on state vectors. Physical properties of a system, known as observables, are represented by Hermitian matrices that satisfy $\boldsymbol{O}^\dagger = \boldsymbol{O}$, where $\dagger$ is the conjugate transpose.

Measurement in matrix mechanics is very different from measurement in classical mechanics. In the latter, the outcome of a measurement can be deterministically predicted if the state of the system being measured is known. In contrast, despite the fact that a quantum system's state is completely determined by the vector $|\Psi\rangle$, measuring a property $\boldsymbol{O}$ can lead to many outcomes, given by the eigenvalues of the matrix $\boldsymbol{O}$. As will be shown below, $|\Psi\rangle$ only determines the relative probability of obtaining a particular outcome. Even more striking, $|\Psi\rangle$ is changed by the measurement process, to the eigenstate corresponding to the measurement outcome:

$$|\Psi\rangle \rightarrow |o\rangle \tag{1.1}$$

where $\boldsymbol{O}|o\rangle = o|o\rangle$, thus indicating that the measurement outcome is o. The arrow represents the *collapse* of the state during the measurement process, which can be understood in the following way. One can always write $|\Psi\rangle = \sum_i o_i |o_i\rangle$, since the eigenstates $\{|o_i\rangle\}$ of an observable $\boldsymbol{O}$ form an orthonormal basis in

$\mathscr{H}$. As such, Eq. 1.1 is saying that a measurement of $\boldsymbol{O}$ always changes the measured state to one of the eigenstates of $\boldsymbol{O}$. Unless $|\Psi\rangle$ itself is an eigenstate of $\boldsymbol{O}$, it is impossible to deterministically predict the measurement outcome o, nor how the state is affected by the measurement. This marks a considerable departure from classical mechanics: the measurement process *disturbs* the state if it is not one of the eigenstates of the measured quantity, and the measurement outcome can only be predicted probabilistically through the Born rule: $\text{Prob}(o) = |\langle o|\Psi\rangle|^2$.

This measurement-induced disturbance also implies that certain quantities can never be measured together precisely, in particular those that do not share eigenstates. To demonstrate this, consider two observables $\boldsymbol{O}$ and $\boldsymbol{P}$ that do not share eigenstates, and a system initially in $|o\rangle$, one of the eigenstates of $\boldsymbol{O}$. First, we measure $\boldsymbol{O}$: $|o\rangle \rightarrow |o\rangle$. As expected, the measurement simply yields the outcome o with certainty, since $\text{Prob}(o) = |\langle o|o\rangle|^2 = 1$, and leaves the state of the system as $|o\rangle$. However, a subsequent measurement of $\boldsymbol{P}$: $|o\rangle \rightarrow |p\rangle$ yields the result p with probability $\text{Prob}(p) = \left|\langle o|p\rangle\right|^2$, and collapses the state. Now reverse the measurement sequence. A first measurement of $\boldsymbol{P}$ yields a result p *and* collapses the state, *i.e.* $|o\rangle \rightarrow |p\rangle$. As such, a subsequent $\boldsymbol{O}$ measurement now yields an outcome which cannot be predicted with certainty, even though the system was initially prepared in one of its eigenstates. Put more succinctly:

$$\boldsymbol{OP}\,|o\rangle \neq \boldsymbol{PO}\,|o\rangle\,, \tag{1.2}$$

which can be interpreted as saying that the measurement of one observable disturbs the measurement of another observable if they do not share eigenstates. Observables such as $\boldsymbol{O}$ and $\boldsymbol{P}$ are known as *incompatible* or *non-commuting*, because they satisfy the mathematical property:

$$[\boldsymbol{O},\boldsymbol{P}] \equiv \boldsymbol{OP} - \boldsymbol{PO} \neq 0 \tag{1.3}$$

where $[\boldsymbol{O},\boldsymbol{P}]$ is a *commutator*. The fact that certain observables do not commute led the founding figures of quantum mechanics to begin questioning the limits in the precision with which non-commuting properties could be determined simultaneously. In particular, they focused on *complementary* properties, which can be defined as properties which are the most incompatible (or have the largest commutator), like position and momentum. This is discussed further below.

Slightly after matrix mechanics, Schrödinger's wave mechanics emerged. There, instead of being a vector, the state of a general quantum system is described by a *wave function*, *e.g.* $\Psi(x)$. As its name suggests, wave mechanics is

founded on de Broglie's idea that all microscopic particles have wave-like properties. For instance, their wavelength depends on their momentum, $\lambda = h/p$, where h is Planck's constant. Furthermore, as with all waves, they obey a wave equation known as Schrödinger's equation which governs their dynamics. Owing to their wave dynamics, quantum particles can interfere with each other and even themselves, perhaps best depicted by the double-slit experiment with electrons. Less obviously, they must also obey an uncertainty principle to reconcile their wave-particle duality. On the one hand, as particles, they are localized in space. On the other hand, a wave can only be localized if it is made up of multiple wavelengths (*i.e.* a wavepacket). This spread in wavelength gives rise to a spread in momentum. Conversely, a wave can have a well defined wavelength, but then must be delocalized. This trade-off is a purely classical wave phenomena, and can be understood as being a consequence of the Fourier transform [19]. Since quantum particles exhibit a wave-particle duality, this uncertainty principle, which would ordinarily only apply to waves, also applies to quantum particles [1].

Heisenberg realized this fact first, and so has the honor of having the following uncertainty principle named after him:

$$\Delta x \Delta p \geq \hbar/2, \tag{1.4}$$

where $\Delta x = \sqrt{\langle \boldsymbol{x^2} \rangle - \langle \boldsymbol{x} \rangle^2}$ and $\Delta p = \sqrt{\langle \boldsymbol{p^2} \rangle - \langle \boldsymbol{p} \rangle^2}$ is the spread in the position and momenta of a quantum particle (that depends on its state), and $\hbar = h/2\pi$. In fact, Heisenberg's uncertainty principle can be understood using both matrix mechanics and wave mechanics. In the former, non-commuting observables, such as position and momentum, do not have simultaneous eigenstates and thus cannot be defined precisely simultaneously. In the latter, quantum particles are wave-like, and thus must satisfy an uncertainty principle. In both cases, it is crucial to understand that the uncertainty principle is an *intrinsic* property of any quantum system [66, 81]. Not long after Heisenberg, Robertson showed that a similar relation exists for any two non-commuting observables $\boldsymbol{A}$ and $\boldsymbol{B}$ [80]:

$$\Delta \boldsymbol{A} \Delta \boldsymbol{B} \geq \frac{1}{2} |\langle [\boldsymbol{A}, \boldsymbol{B}] \rangle| . \tag{1.5}$$

[1] This idea of an uncertainty principle arising from the wave-particle duality of quantum particles can be extended to other systems. All quantum systems have *complementary* properties, such as energy and time, or spin along z and spin along x, that also give rise to this uncertainty.

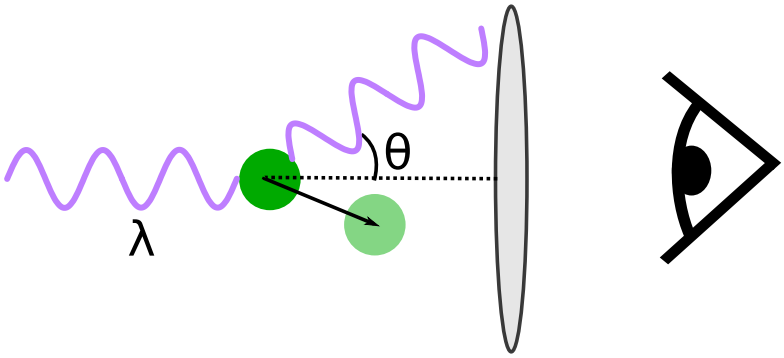

Figure 1.2: The gedankenexperiment of Heisenberg. Gamma rays illuminate an electron to measure its position. The rays are collected by a lens and focused on a detector. Due to Compton scattering, the act of measuring the electron's position causes a disturbance in its momentum.

Heisenberg, however, explained his uncertainty principle in a different manner with his famous microscope gedankenexperiment [37]. In it, the goal is to determine the position of an electron using a gamma ray microscope, as shown schematically in Fig. 1.2. Gamma rays are illuminated on an electron. A lens then collects the rays and focuses them onto an observer. Classical optics dictates that diffraction of the light limits the precision with which the electron's position can be resolved:

$$\Delta x = \lambda / \sin\theta, \tag{1.6}$$

where λ is the wavelength of the light and θ is the opening angle (or $\sin\theta$ the numerical aperture) of the lens. Microscopically, a different effect occurs. Photons scatter off the electron, thus disturbing its position. This process is described by Compton scattering, which predicts a change in momentum of the electron:

$$\Delta p = h \sin\theta / \lambda, \tag{1.7}$$

from which we deduce $\Delta x \Delta p \sim h$, roughly similar to Eq. 1.4. Thus, the act of measuring the position of the electron disturbs its momentum due to the measurement apparatus. In fact, measurement-induced disturbance is a general phenomenon known as the *observer effect*, and can occur in other areas of physics, such as in electronics and thermodynamics [2]. In this gedankenexperiment, Heisenberg's intention is to explain the uncertainty principle as a

[2] In electronics, an ideal voltmeter is assumed to have an infinite resistance. In practice, the voltmeter draws some current, and thus the presence of the voltmeter affects the voltage

consequence of measurement disturbance. Interestingly, this explanation still depends on the wave-particle duality of light.

The microscope gedankenexperiment raises an important question: is it possible to design a measurement that does not disturb the momentum of the electron in the process of making a position measurement? As it turns out, the answer to this question is yes, to some extent. These types of measurements are the subject of this thesis. If achieved, then non-commuting and even complementary properties can be measured simultaneously in what is known as a *joint measurement* [3]. Although joint measurements circumvent measurement disturbance, they cannot circumvent the uncertainty principle. The latter is an intrinsic property of quantum systems which exists irrespective of the measurement strategy.

1.2 What is *not* a joint measurement

Before proceeding further, it is worth clarifying what is meant by a joint measurement by providing non-examples. The goal is to devise a strategy to simultaneously measure two non-commuting properties of a system in state $|\psi\rangle$, namely its position $\boldsymbol{x}$ and momentum $\boldsymbol{p}$. It is implicit that one has access to an ensemble of identical copies of the system being measured. In this way, the measurement can be repeated to build statistics and determine expectation values such as $\langle x\rangle$ and $\langle p\rangle$.

Two naive strategies are shown in Fig. 1.3. Thanks to our earlier discussion about collapse, the first can already be ruled out. Namely, a copy of $|\psi\rangle$ is taken out of the ensemble, one at a time, and the non-commuting properties are sequentially measured. An initial $\boldsymbol{x}$ measurement collapses the state to a position eigenstate, $|\psi\rangle \rightarrow |x\rangle$ with probability $\text{Prob}(x) = \left|\psi(x)\right|^2$. Because of the collapse, subsequent momentum measurements do not depend on $|\psi\rangle$ and yield

being measured. Similarly, thermodynamics dictates that a standard mercury thermometer must exchange some heat in order for the mercury level to change. This heat exchange affects the temperature of the body the thermometer is measuring. Granted, both these effects are so small that they can be neglected in practice. However, the point is that, it is not so uncommon that measurements are disturbing, even outside quantum physics.

[3] Here, the term joint measurements is referring to those that simultaneously measure non-commuting properties on single quantum systems. The term is sometimes also used to describe a measurement on composite systems. In that case, non-commuting properties are simultaneously measured on different subsystems, such as two particles in an entangled state. This second type of joint measurement is required for testing Bell's inequalities.

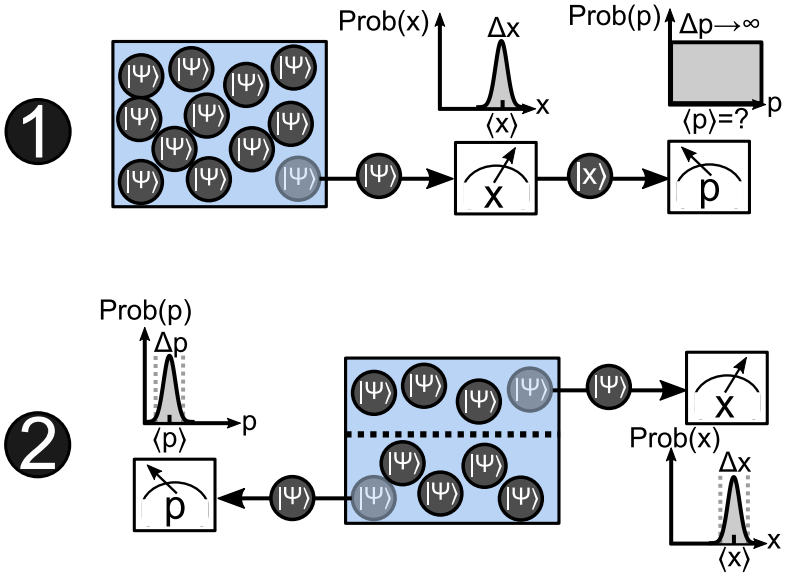

Figure 1.3: Naive strategies for performing joint measurements. The first strategy fails, since the momentum measurement yields random results. The second strategy fails, since the position and momentum measurements are independent and so there cannot be correlations between the results.

random results, *i.e.* $|x\rangle \rightarrow |p\rangle$ with a probability that does not depend on p. Thus nothing is learned about the system's momentum.

A slightly more clever strategy is to take two copies of $|\psi\rangle$ out of the ensemble at a time, and simultaneously measure $\boldsymbol{x}$ on one copy, and $\boldsymbol{p}$ on the other. Since the measurements are performed on two separate copies, they do not disrupt each other as in the sequential strategy. By keeping track of the relative fraction of measurement trials resulting in a particular outcome, one can determine probability distributions $\text{Prob}(x)$ and $\text{Prob}(p)$. The center of these distributions is the expectation value of the measured property. Assuming one uses very precise measurement devices, the spread in these distributions is the intrinsic uncertainty of these properties which depends on the state $|\psi\rangle$, *e.g.* $\Delta x = \sqrt{\langle\psi|\boldsymbol{x^2}|\psi\rangle - \langle\psi|\boldsymbol{x}|\psi\rangle^2}$. One could argue that this strategy successfully simultaneously determined $\boldsymbol{x}$ and $\boldsymbol{p}$ of the system. While this is true, it is not a valid joint measurement. The issue with this strategy lies with the fact that the measurements of $\boldsymbol{x}$ and $\boldsymbol{p}$ are independent, and as such, their outcomes are not correlated. In other words, the *joint* probability of obtaining a particular outcome (x, p) is simply the probability of measuring x multiplied by the probability of measuring p: $\text{Prob}(x, p) = \text{Prob}(x)\text{Prob}(p)$. The reason that this is an issue is that the system could have correlations between its position and momentum. For example, this would the case if there were an expanding gas in the blue box. This measurement strategy fails to be sensitive to these correlations, since the joint probability distribution is always factorable. As such, it is an invalid joint measurement. In this thesis, we define a valid joint measurement as one where, if complementary properties (*e.g.* $\boldsymbol{x}$ and $\boldsymbol{p}$) are being jointly measured, then the joint measurement should be able to determine the system's state (see Sec. 1.4).

1.3 Development of joint measurement strategies

How, then, could we ever jointly measure the position and momentum of a quantum system, *while* still being sensitive to correlations between these properties? This question is a difficult one, and it took physicists a long time to answer. Perhaps the missing ingredient was a more general formalism to describe measurement than what was offered by the early matrix or wave mechanics. In particular, von Neumann was not content with the collapse pictured offered by these formalisms. The arrow in Eq. 1.1 seems like a mere mathematical convenience, instead of being representative of an actual physical mechanism during

the measurement process. Indeed, this is an open problem even today, known as the *measurement problem*, and is a topic too daunting to broach in this thesis. Nevertheless, von Neumann studied it extensively in his 1932 book "Mathematical foundations of quantum theory" [95]. In doing so, he developed a more general formalism for treating measurement, including *projector operator valued measures* (POVMs) and *indirect measurement*, the latter of which is described in more detail in Sec. 2.1.

The more general measurement formalism of von Neumann eventually led to the development of strategies for performing joint measurements. However, this did not happen immediately. More than thirty years after his book was published, in 1965, Arthurs and Kelly wrote a seminal paper on simultaneously measuring the position and momentum of a particle with a precision that saturates the uncertainty principle [5]. Their idea was based on von Neumann's indirect measurement: the measured particle is coupled to a *pointer* system, and the measurement result is read-out by probing the pointer instead of the particle [4]. The Arthurs-Kelly scheme required two pointers, one for position and one for momentum. It remains to this day a useful toy model for a valid joint measurement strategy.

Another important contribution to the development of joint measurements came from a very different perspective. In the 1980s, scientists were designing the Light Interferometer Gravitational-Wave Observatory (LIGO), a 4 km long interferometer whose aim was to resolve optical path length differences as small as 10^{-20} m. With such a precision, they were hoping to measure fluctuations in space-time caused by gravitational waves [5]. Evidently, this proposed experiment was verging on the fundamental limits of measurement precision. Concurrently, Braginsky, Voronstov, and Thorne wrote a seminal paper on how to beat the *standard quantum limit* of measurement precision to improve the sensitivity of LIGO [12]. The idea behind this limit is that a very precise position measurement will assuredly disturb the system's (*e.g.* the mirror in an interferometer) momentum, as in Heisenberg's microscope. After some time, this momentum disturbance will in turn disturb the system's position. They coined this effect *back-action*. In their paper, Braginsky *et al.* proposed the idea of *non-demolition measurements*, which minimized back-action using tech-

[4] This is the quantum analogue of something we often encounter in measurement. For example, we determine the intensity of light hitting a photodiode by measuring the current it outputs. Thus, the current is a pointer for the measured system, the light intensity.

[5] Hope became reality in 2016, when the LIGO collaboration announced that they detected gravitational waves generated by two merging black holes.

niques similar to indirect measurement. Quite recently, this idea has been used to implement joint measurements [34, 20].

Eight years later, in 1988, another contribution was made by Aharanov, Albert and Vaidman in their seminal paper: "How the result of a measurement of a component of the spin of a spin-1/2 particle can turn out to be 100" [3]. This provocative title referred to a rather provocative idea: that a system could be measured without disturbing its state. This is now known as a weak measurement, and can be achieved with von Neumann's indirect measurement, but using a very weak coupling between system and pointer. Since weak measurements hardly disturb the state, non-commuting observables can be measured sequentially without disrupting each other, thus enabling joint measurements. This is discussed in further detail in Ch. 2. In addition to introducing the idea of weak measurements, the 1988 paper introduced the idea of weak value amplification: how keeping only certain outcomes in a weak measurement could be useful for metrology in quantum physics. In recent years, these ideas are still being used to achieve tremendously precise measurements [26], and the foundational implications of their work is still being debated [47, 28].

Recently, in 2012, another joint measurement strategy was devised by Holger Hofmann [38]. It is fundamentally different than that previously mentioned strategies in that, instead of modifying how the measurement is performed (*e.g.* weak or non-demolition measurements), the system being measured is manipulated. In particular, Hofmann showed that producing quantum clones of a system and measuring a non-commuting observable on each clone is a valid joint measurement strategy. This is discussed in detail in Ch. 4 and Ch. 5.

As can be seen, the development of joint measurements was a rather slow one. Over the course of the 20th century, theorists continued to investigate the concept of simultaneous measurements of non-commuting observables. Ultimately, this investigation led to non-demolition and weak measurements. Both of these strategies have recently been achieved experimentally [55, 34], which has renewed an interest in joint measurements. For example, in a series of debated works, they have been used to show that Heisenberg's gedankenexperiment explanation of the uncertainty principle is not universal and can be violated [81, 66, 16]. Joint measurements have also found application in quantum metrology as ultra-precise measurements [26, 20]. In parallel to all of this work, others were thinking about joint measurements from a completely different perspective: how they can be useful for quantum state determination. This is the subject of the next section.

1.4 Joint measurement and phase-space

Classical physics can be formulated in phase-space. There, the state of a system such as a single particle is completely specified by its conjugate properties, *e.g.* (x, p). The dynamics of the particle can be determined using only these numbers and its equations of motion. More generally, systems can also be comprised of particles in statistical ensembles, which is the case for an ideal gas. Instead of a pair of numbers, the state of such systems is described by a joint probability distribution $\text{Prob}(x, p)$, known as a phase-space distribution. The dynamics and properties of these distributions is the subject of statistical mechanics. Like the single particle case, phase-space distributions have an intuitive physical meaning: $\text{Prob}(x, p)$ is the probability for a particle in the ensemble to have a position x and momentum p. This meaning also readily provides a method for measuring the state of a general system in classical physics: determine $\text{Prob}(x, p)$ by jointly measuring the relative fraction of particles in the statistical ensemble that have a position x and momentum p.

In quantum mechanics, the uncertainty principle forbids precise and simultaneous knowledge of x and p. This complicates things quite a bit, and indeed, standard joint probability distributions are no longer valid for describing quantum states. Not long after the inception of quantum mechanics, in 1932, Wigner extended the phase-space formalism to quantum systems by finding quantum corrections to statistical mechanics [96]. He found that a quantum state $\psi(x)$ has the following "Wigner function":

$$W(x, p) = \frac{1}{\hbar\pi} \int_{-\infty}^{\infty} dy \psi(x + y)\psi^*(x - y)e^{2ipy/\hbar}. \tag{1.8}$$

Like a classical phase-space distribution, $W(x, p)$ fully describes the state of a quantum system in terms of only its conjugate (or complementary) properties, but while still satisfying the uncertainty principle. In other words, it is an equivalent description of the state to $\psi(x)$. However, $W(x, p)$ can have negative values, and as such, is not a valid joint probability distribution like the classical $\text{Prob}(x, p)$. Instead, $W(x, p)$ is referred to as a *quasiprobability distribution*. After the work of Wigner, a zoo of other quasiprobability distributions emerged [25, 59, 46, 7]. They are all equivalent in that they contain the same information as $W(x, p)$ and $\psi(x)$, just represented differently. However, in all cases, they have features that prevent them from being valid (*i.e.* satisfying Kolmogorov axioms) probability distributions. Evidently, this is a consequence of the uncertainty principle. Eventually, in 1949, Moyal derived a theory com-

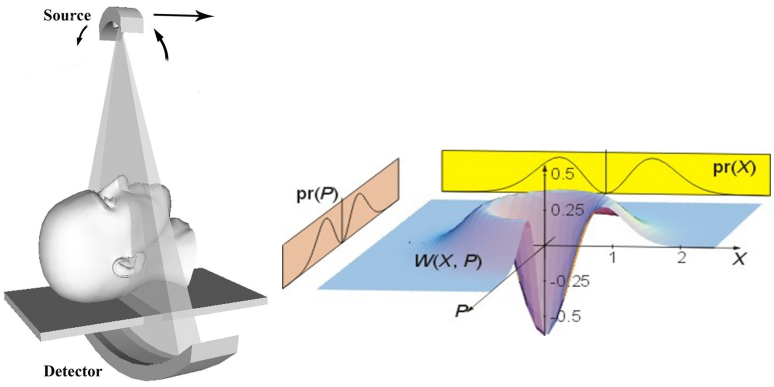

Figure 1.4: The idea of quantum state tomography was inspired by medical X-ray tomography. Instead of imaging slices of the brain (left), the marginals of the quasiprobability distribution $W(x,p)$ (right) are measured. With a sufficient amount of marginals, the entire $W(x,p)$ can be tomographically reconstructed. Image credits in Ref. [1].

pletely equivalent to conventional quantum mechanics where everything (*i.e.* states, measurement, dynamics) is described in phase-space [62]. Thus, Moyal showed that both classical and quantum physics can be formulated in a common formalism. Because of this, phase-space distributions continue to be an essential tool to study the transition between the two theories and to identify strictly non-classical phenomena.

One of the issues with quasiprobability distributions is their physical meaning. In contrast to classical probability distributions, $W(x,p)$ can no longer be interpreted as being the probability for a system to have a position x and momentum p, since it goes negative. As such, it is not clear how it could be measured. However, it is important to note that there was similar confusion with the conventional description of the quantum state, the wave function $\psi(x)$. Indeed, after Schrödinger's wave mechanics was developed, Pauli famously questioned the measurability of the wave function [71]. To Pauli, it was not clear if the only measurable quantity was the probability $|\psi(x)|^2$, instead of the probability amplitude $\psi(x)$. Furthermore, if the answer to his question was the latter, could $\psi(x)$ ever be measured for a single particle, or only for an ensemble? For a long time, this question was left unanswered.

Remarkably, the answer came from the world of medicine. Medical doctors were using x-rays to image the brain (see Fig. 1.4). Their method, which was

recognized by the 1979 Nobel prize in Medicine, was based on measuring many cross-sections of the brain, and tomographically reconstructing a 2D image using a mathematical tool known as the Radon transformation. Similarly, physicists realized that, although the Wigner function cannot be measured point-by-point, it could be reconstructed tomographically from its marginals, *e.g.* $\text{Prob}(x) = \int_{-\infty}^{\infty} dp W(x,p) = |\psi(x)|^2$. Each marginal (a projection of $W(x,p)$ onto a particular axis in (x,p) space) is determined via the Born rule by performing many measurements on identically prepared copies of the system. Several experimental techniques already existed to measure a sufficiently complete set of marginals in a variety of systems, notably Stokes polarimetry for polarization and homodyne for quantum states of light [89].

This was the birth of quantum state tomography, a tool which is now used every day by experimental physicists to determine unknown quantum states. Since $W(x,p)$ is equivalent to the wave function $\psi(x)$, it is possible to extract the latter from the former. As such, tomography answered Pauli's question about the measurability of $\psi(x)$: it *is* possible to measure $\psi(x)$, albeit indirectly. Furthermore, the reconstruction requires the use of an ensemble of identical copies of the state [75]. For a long time, tomography was the only measurement procedure that could be used to measure a quantum state. Unfortunately, it does not ascribe a satisfying physical meaning to the state. The procedure is indirect in that the measurement result does not correspond to the value of the state at a particular point. Furthermore, tomography is inefficient since the inverse problem of reconstructing $W(x,p)$ from its marginals is a hard one: the reconstruction algorithms are slow, and often the dataset used to perform the reconstruction is overcomplete (*i.e.* contains redundant information). Ideally, the wave function can be determined at a desired point $\psi(x)$, and the measurement results are directly related to the probability amplitude. It turns out that joint measurements provide a way to this.

Since joint measurements can simultaneously determine *e.g.* x and p, one would expect them to be connected in some way to phase-space distributions such as $W(x,p)$. Surprisingly, although quasiprobability distributions and joint measurements were thoroughly studied independently, the connection between the two was not. After the seminal paper of Arthurs and Kelly, a few early works explored the possibility of using joint measurements to determine quasiprobabilities [85, 69, 23], but never arrived at a conclusive answer. It was not clear how to relate the relative frequency of obtaining a particular joint measurement outcome to a negative or even complex quantity. However, joint measurements can determine products of non-commuting Hermitian operators,

e.g. $\boldsymbol{xp}$, which may not be Hermitian and thus may have complex eigenvalues, *i.e.* measurement outcomes. To the best of my knowledge, no early work provided a method to determine a quasiprobability distribution with a joint measurement. Instead, a convincing answer came from Leonhardt and Paul in 1993, who realized that eight-port homodyne can be used to directly determine a quasiprobability distribution known as the Q-function of a quantum state of light [50]. While the aforementioned homodyne measures a single marginal at a time, eight-port homodyne (essentially two homodyne setups) simultaneously measures both quadratures $\boldsymbol{x}$ and $\boldsymbol{p}$ of the electromagnetic field [64]. Since then, other joint measurement methods have been used to perform *direct measurement* of the state of a system. That is, quasiprobability distributions [50, 6, 82], the wave function $\psi(x)$ [55], and even the density matrix (see Ch. 3), *can* be measured point-by-point, as would be done classically. The key is to jointly measure complementary properties of the system.

Direct measurement is of great importance for the foundations of quantum physics, since it provides an *operational* definition to quantum states, *i.e.* defined by an experimental procedure that provides the value of the state at a given point. Moreover, it has several practical advantages over tomography in terms of efficiency. Throughout the remainder of the thesis, I discuss in more details how joint measurements can be used to directly measure quantum states and their advantages over tomography. It is important to realize that, even with direct measurement, the quantum state is not a measurable quantity with only a single particle, since the joint measurement result must still be averaged over many trials. In fact, it has been proven that it is impossible to measure the state of a single quantum particle [22].

1.5 Summary

The development of joint measurements progressed as physicists gradually refined their understanding of foundational concepts in quantum physics, such as the Heisenberg uncertainty principle, non-commuting observables, and measurement disturbance. Throughout the 20th century, joint measurements were studied by physicists that can be categorized into two camps. One camp was investigating measurements strategies that could circumvent measurement disturbance. Thanks to von Neumann's generalized measurement formalism, this investigation led to the Arthurs-Kelly scheme, non-demolition measurements, and weak measurements. The other camp was interested in a phase-space for-

mulation of quantum mechanics. This led to the first convincing proposal to determine quasiprobabilities distributions with a joint measurement, namely using eight-port homodyne to simultaneously measure complementary quadratures of the electromagnetic field. Thus, this second camp showed that joint measurements could be used to directly measure quantum states, instead of tomographically.

Chapter 2

Weak measurement

In this chapter, I present the topic of weak measurements. These were introduced by Albert, Aharonov, and Vaidman in 1988 [3]. They are based on a simple idea: if a normal measurement collapses the state, can we perform a "gentle" measurement that leaves the state unchanged? In that way, one could measure other non-commuting properties afterwards. Indeed, I will show that this is a valid joint measurement strategy.

2.1 Indirect measurement

Indirect measurement was devised by von Neumann in 1932 [95] in an attempt to develop a more general and realistic description of measurement than what was offered by matrix and wave mechanics. Today, it is of paramount importance in quantum physics. For instance, it paved the way to the first joint measurement scheme of Arthurs and Kelly. Besides that, indirect measurement plays a central role in decoherence theory, which is regarded as being a candidate for, maybe one day, solving the measurement problem.

Many physicists are probably already familiar with indirect measurements. Undergraduate students often begin their first quantum mechanics course with the Stern-Gerlach experiment, which is depicted in Fig. 2.1. Its aim is to determine the spin of the valence electron of silver atoms, which is achieved by sending the atoms through an inhomogeneous magnetic field $B(z) = \lambda z$ [1]. This field deflects the atoms either up or down, depending on their spin, as it inter-

[1] This assumes the magnetic field is very weak along other axes as to not violate Maxwell's equations, *i.e.* $\nabla \cdot B = 0$

acts with the magnetic dipole moment of the valence electron. Thus, by looking at where the atoms land on a detector, their spin can be measured. Stated this way, it is clear that this is an indirect measurement. The spin of the atoms is not measured directly. Instead, it is inferred from a position measurement.

Formally, the Stern-Gerlach experiment can be described as follows. The full state of the atom is comprised of two degrees of freedom: a spin state $|s\rangle$ (*system*) and a spatial state $|\chi\rangle$ (*pointer*). Before any measurement, these are not correlated, and so the total initial state of the atoms is $|\Psi_i\rangle = |s\rangle \otimes |\chi\rangle$. We suppose that the spin state is arbitrary but quantized along $\hat{z}$:

$$|s\rangle = c_\uparrow |\uparrow\rangle + c_\downarrow |\downarrow\rangle, \tag{2.1}$$

where $|c_\uparrow|^2 + |c_\downarrow|^2 = 1$. The exact spatial state of the atoms $|\chi\rangle$ would depend on the details of the source of the atoms, *e.g.* an oven's aperture. For simplicity, we can assume it is a localized function like a Gaussian of width σ:

$$\langle z|\chi(z)\rangle = \chi(z) = \frac{1}{\sqrt{2\pi}\sigma} e^{-z^2/2\sigma^2}. \tag{2.2}$$

As the atoms pass through the magnetic field, their spin and position interact according to the interaction Hamiltonian:

$$\mathscr{H}_{int} = \lambda \mu_B \boldsymbol{S_z z}. \tag{2.3}$$

Here, $\lambda = \partial B/\partial z$ dictates the strength of the interaction and can be tuned with the magnetic field strength, while $\mu_B = e\hbar/2m_e$ is the Bohr magnetron. The effect of this interaction on the atoms is found by time-evolving their total state:

$$\begin{aligned} |\Psi(t)\rangle &= e^{-i\mathscr{H}_{int}t/\hbar}(|s\rangle \otimes |\chi(z)\rangle) \\ &= e^{-i\lambda\mu_B \boldsymbol{S_z} z t/\hbar}\left((c_\uparrow |\uparrow\rangle + c_\downarrow |\downarrow\rangle) \otimes |\chi(z)\rangle\right) \\ &= c_\uparrow |\uparrow\rangle\, e^{-i\lambda\mu_B z t/2} |\chi(z)\rangle + c_\downarrow |\downarrow\rangle\, e^{i\lambda\mu_B z t/2} |\chi(z)\rangle. \end{aligned} \tag{2.4}$$

The operator $e^{\pm i\lambda\mu_B z t/2}$ is the generator of translations of momentum [2], and causes the atom's momentum to be shifted by an amount $\pm\lambda\mu_B t/2$. Thus, it imparts a positive impulse to $|\uparrow\rangle$ spin atoms, and a negative impulse to $|\downarrow\rangle$ spin

[2] It is also common to couple the observable of interest $\boldsymbol{A}$ to the pointer momentum operator $\boldsymbol{p}$ instead of the position operator, *i.e.* $\mathscr{H}_{int} = g\boldsymbol{Ap}$, where g is the strength of the coupling. In that case, the unitary operator corresponding to the interaction Hamiltonian is the generator of translations of position. This is the case in Ch. 3. The idea remains the same, however.

atoms, as depicted in Fig. 2.1. Once the atoms reach the detector screen, they will have a position that depends on the strength of this impulse. Avoiding superfluous details, the total state just before detection is:

$$|\Psi_f\rangle = c_\uparrow |\uparrow\rangle |\chi(z-\lambda z_0)\rangle + c_\downarrow |\downarrow\rangle |\chi(z+\lambda z_0)\rangle\,, \tag{2.5}$$

where z_0 is a constant that depends on the distance between the magnetic field and the detector, the spatial extent of the magnetic field along the x axis, the average kinetic energy of the atoms, and fundamental constants.

So what was the point of this calculation? Eq. 2.5 exhibits the essence of indirect measurement: A *pointer* (spatial state of atom) is coupled to a *system* (spin state of atom) through an interaction that depends on the observable being measured ($\boldsymbol{S_z}$). This interaction causes the pointer to be shifted by an amount proportional to the outcome of the measurement (*i.e.* one of the eigenvalues of $\boldsymbol{S_z}$). Then, the indirect measurement is resolved by determining the average shift of the pointer:

$$\begin{aligned}\langle \boldsymbol{z}\rangle &= \langle\Psi_f|\boldsymbol{z}|\Psi_f\rangle \\ &= |c_\uparrow|^2 \langle\chi(z-\lambda z_0)|\boldsymbol{z}|\chi(z-\lambda z_0)\rangle + |c_\downarrow|^2 \langle\chi(z+\lambda z_0)|\boldsymbol{z}|\chi(z+\lambda z_0)\rangle \\ &= \lambda z_0(|c_\uparrow|^2 - |c_\downarrow|^2) \\ &\propto \langle \boldsymbol{S_z}\rangle\,.\end{aligned} \tag{2.6}$$

Note that the average pointer shift is only *proportional* to the observable expectation value in this case, since $\langle s|\boldsymbol{S_z}|s\rangle = \hbar/2(|c_\uparrow|^2 - |c_\downarrow|^2)$. This shows that it is important to understand the experimental apparatus in full detail (*i.e.* details of z_0) to find the conversion between observable eigenvalue and pointer position. These details are typically glossed over when the Stern-Gerlach experiment is presented, and yet, the concept of indirect measurement is ubiquitous in physics.

2.2 Weak measurement

The state in Eq. 2.5 is entangled. This is why the measurement result of the atom's position is correlated to its spin. It also means that, measuring its position disturbs its spin state. Suppose $\lambda z_0 \gg \sigma$, meaning the pointer shift is much larger than its width. In this *strong measurement* limit, the pointer states of each measurement outcome hardly overlap, *i.e.* $\langle\chi(z+\lambda z_0)|\chi(z-\lambda z_0)\rangle \approx 0$,

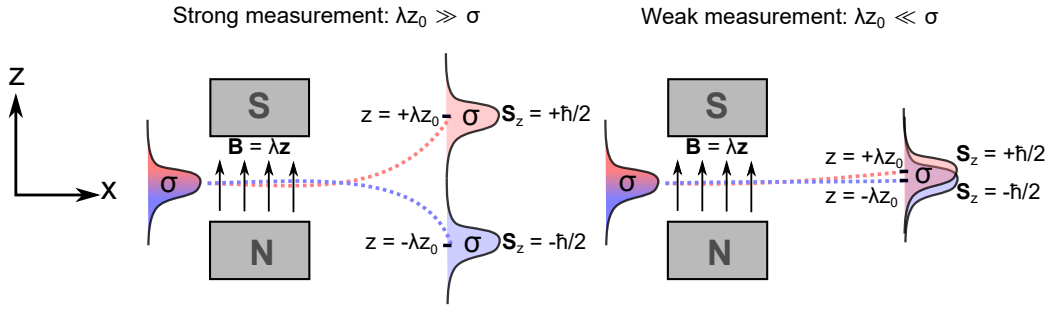

Figure 2.1: The Stern-Gerlach experiment can be treated using von Neumann's indirect measurement formalism. The magnetic field entangles the spin of atoms with their position. If a strong field is used, a position measurement unambiguously determines the spin of the atoms, but disturbs the spin state of the atoms. If a weak field is used, one trades-off measurement disturbance for information gained in a single trial.

and so a measurement of the pointer position collapses the spin state of the atom, *e.g.* $\langle\chi(z-\lambda z_0)|\Psi_f\rangle \approx |\uparrow\rangle$. This is ideal if one wants to determine the spin of the atom in a single trial.

In contrast, in the weak measurement limit, $\lambda z_0 \ll \sigma$, and so the two pointers almost completely overlap on the detector, *i.e.* $\langle\chi(z+\lambda z_0)|\chi(z-\lambda z_0)\rangle \approx 1$. Consequently, the degree of entanglement between the spin and position of the atoms is very small. In that case, measuring their position no longer disturbs their spin state, but does not unambiguously determine the spin of the atom in a single trial. Thus, there is a trade-off between the amount of information gained about the spin in a single measurement trial, and the disturbance that measurement causes to the spin. This trade-off is due to the entanglement between the pointer and the system. The trick in weak measurement is that the loss in information per trial can be compensated by increasing the number of trials. In other words, $\langle \boldsymbol{S_z}\rangle$ can still be found unambiguously, since it is still proportional to $\langle \boldsymbol{z}\rangle$. Crucially, in each trial, measurement disturbance is minimized.

2.3 Sequential weak measurements

2.3.1 Weak value

Because weak measurements can be used to obtain information about an observable with minimal disturbance to the system, it seems natural to use them to perform a sequence of measurements. That way, many observables can be measured, without these measurements disrupting each other. In particular, the observables being measured could be non-commuting, thus enabling joint measurements.

The simplest sequence would be a weak measurement followed by a strong measurement. Although the strong measurement would collapse the state, this is not an issue since no subsequent measurements are performed. Because of its importance in the literature, it is worth saying a few words about the result of this particular measurement sequence. Keeping with the Stern-Gerlach example, suppose one performs a weak measurement of $\boldsymbol{S_z}$ followed by a strong measurement of $\boldsymbol{\pi}_f = |f\rangle\langle f|$, where $|f\rangle$ is some spin state. The strong measurement is performed without a pointer, directly on the system. In that case, the state of the atoms after passing through the magnetic field and the $\boldsymbol{\pi}_f$ measurement is given by:

$$|\Psi(t)\rangle = |f\rangle\langle f| e^{-i\lambda\mu_B \boldsymbol{S_z} \boldsymbol{z} t/\hbar}(|s\rangle \otimes |\chi(z)\rangle). \tag{2.7}$$

In the weak measurement limit, we can expand the translation operator keeping only the first order term, since $\lambda z_0 \ll \sigma$:

$$\begin{aligned} |\Psi(t)\rangle &\approx |f\rangle\langle f| \left(1 - i\lambda\mu_B \boldsymbol{S_z} \boldsymbol{z} t/\hbar\right)(|s\rangle \otimes |\chi(z)\rangle) \\ &= \left(\langle f|s\rangle - \langle f| i\lambda\mu_B \boldsymbol{S_z} \boldsymbol{z} t/\hbar|s\rangle\right)|f\rangle \otimes |\chi(z)\rangle \\ &= \langle f|s\rangle \left(1 - i\lambda\mu_B \langle \boldsymbol{S}_z\rangle_w \boldsymbol{z} t/\hbar\right)|f\rangle \otimes |\chi(z)\rangle \\ &\approx \langle f|s\rangle |f\rangle e^{-i\lambda\mu_B \langle \boldsymbol{S}_z\rangle_w \boldsymbol{z} t/\hbar}|\chi(z)\rangle, \end{aligned} \tag{2.8}$$

where we defined the *weak value*:

$$\langle \boldsymbol{S_z}\rangle_w \equiv \frac{\langle f|\boldsymbol{S_z}|s\rangle}{\langle f|s\rangle}. \tag{2.9}$$

Thus, the total state just before detection is:

$$|\Psi_f\rangle = \langle f|s\rangle |f\rangle |\chi(z - 2\lambda \langle \boldsymbol{S}_z\rangle_w z_0)\rangle, \tag{2.10}$$

where z_0 is defined in the same way as in Eq. 2.5. Indeed, the result looks similar to Eq. 2.5. However, since there is an additional measurement $|f\rangle\langle f|$ on the system, the final spin state has collapsed to $|f\rangle$ with probability $\left|\langle f|s\rangle\right|^2$. As was the case before, the weak measurement sequence is resolved by determining the average position (and now also momentum) shift of the pointer, namely:

$$\langle \boldsymbol{z}\rangle + \frac{i2\sigma^2}{\hbar}\langle \boldsymbol{p}_z\rangle \propto \langle \boldsymbol{\pi}_f \boldsymbol{S}_z\rangle\,, \tag{2.11}$$

where again, the proportionality is due to z_0. Note that $\boldsymbol{\pi}_f$ and $\boldsymbol{S}_z$ may be non-commuting. This is the case if *e.g.* $|f\rangle = c_\uparrow|\uparrow\rangle + ic_\downarrow|\downarrow\rangle$. As a result, the operator $\boldsymbol{\pi}_f\boldsymbol{S}_z$ may be non-Hermitian and have complex eigenvalues. This manifests itself as a complex pointer shift, leading to both a position and momentum shift. The physical origin of this momentum shift is still a debated topic. One reasonable explanation [90] is that it arises due to *back-action*, which is the small but non-zero measurement disturbance of a weak measurement.

There are interesting physical consequences if we post-select on trials where the $\boldsymbol{\pi}_f$ measurement led to the outcome f (*i.e.* ignore the $f = 0$ outcomes). This essentially re-normalizes the state of $|\Psi_f\rangle$, thus getting rid of the term $\langle f|s\rangle$ in Eq. 2.10. In that case, the average shift of the atoms is given by the weak value:

$$\langle \boldsymbol{z}\rangle + \frac{i2\sigma^2}{\hbar}\langle \boldsymbol{p}_z\rangle \propto \langle \boldsymbol{S}_z\rangle_w\,, \tag{2.12}$$

as was pointed out by Albert, Aharonov, and Vaidman (AAV) in 1988 [3]. Remarkably, the denominator of $\langle \boldsymbol{S}_z\rangle_w$ causes the pointer shift to indicate a measurement result that potentially lies outside the eigenvalue range of $\boldsymbol{S}_z$. This *amplification* is most evident when $|f\rangle = c_\downarrow|\uparrow\rangle - c_\uparrow|\downarrow\rangle$, which is orthogonal to $|s\rangle$. In that case, $\langle f|s\rangle = 0$ and the weak value blows up, hence the provocative title of the AAV paper: "How the result of a measurement of a component of the spin of a spin-1/2 particle can turn out to be 100". The trade-off is that the success of this measurement is very small in the $\langle f|s\rangle \to 0$ limit.

The weak value has been used in optical [79], atomic [87], and superconducting physics [45], to cite a few key papers. Because it can lie outside the eigenvalue spectrum of the measured observable, and can also be complex, the weak value has generated controversy regarding its importance in quantum physics. A comprehensive review on the topic can be found in Ref. [28]. To very briefly discuss one actively researched subtopic, the usefulness of weak value amplification (WVA) in metrology applications is still being debated. While

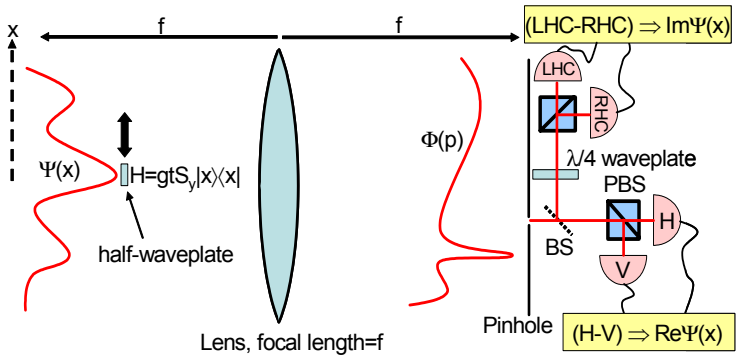

Figure 2.2: Direct measurement of photon's transverse wave function. The measurement sequence consists of a weak position measurement followed by a strong momentum measurement. The resulting pointer shift is a complex polarization shift. Its real part is determined by measuring intensity differences in the linear polarization basis (H: horizontal, V: vertical). Similarly, its imaginary part is determined by measuring intensity differences in the circular polarization shift (RHC: right-hand circular, LHC: left-hand circular). These measurements are directly proportional to the real and imaginary parts of the wave function, respectively. Figure taken from J. Lundeen's PhD thesis (2006).

some experimentalists claimed to have used WVA to measure beam shifts as small as 14×10^{-15} m [26] [3], others claim post-selection is effectively throwing away information, which cannot possibly give a metrological advantage. For readers interested in this topic, see the recent review in Ref. [47].

2.3.2 As a joint measurement: direct measurement

Notably, if the second strong measurement is complementary to the first weak measurement, the weak value is directly proportional to the wave function of the system being measured. This is the type of joint measurement that was discussed in Sec. 1.4. The idea was proposed and experimentally demonstrated by Lundeen *et al.* in 2011 [55]. In their experiment (see Fig. 2.2), they measure the transverse spatial wave function of a photon by first weakly measuring the

[3] This is a truly remarkable feat given that their experimental setup consists of a simple tabletop interferometer. As a comparison, the arms of LIGO are 4 km long, and can resolve 10^{-20} m displacements.

photon's position $\boldsymbol{\pi}_x = |x\rangle\langle x|$, followed by a strong measurement of its momentum $\boldsymbol{\pi}_p = |p\rangle\langle p|$. As a pointer for the weak measurement, they use the photon's polarization degree of freedom. That is, the photon's polarization is weakly coupled to its position using a small birefringent crystal. Their strong momentum measurement is implemented by focusing the photon with a lens and placing a pinhole at the focal plane of the lens. This pinhole transmits only one momentum component of the photon. It is straightforward to check that the average result of this measurement sequence gives the wave function. Indeed, using Eq. 2.9, the average pointer shift is:

$$\frac{\langle p|\boldsymbol{\pi}_x|\psi\rangle}{\langle p|\psi\rangle} = \frac{\langle p|x\rangle\langle x|\psi\rangle}{\langle p|\psi\rangle} = \frac{e^{ipx/\hbar}\psi(x)}{\tilde{\psi}(p)}. \tag{2.13}$$

The authors make the particular choice of choosing $p = 0$ as their post-selection, which is simply fixes a phase reference for the wave function. In that case, the polarization of the photons is shifted by $\psi(x)/\tilde{\psi}(0)$, which is exactly the value of the wave function (the denominator can be eliminated through normalization). Since $\psi(x)$ is complex, the polarization shift is also a complex quantity. The real and imaginary parts can be obtained by measuring the shift in the linear and circular polarization bases, respectively.

The *direct measurement* method of Lundeen *et al.* is a completely novel method for determining the wave function of an arbitrary system. In contrast to tomography, the measurement results correspond directly to the wave function, which can now be measured point-by-point instead of globally reconstructed. It also provides an operational definition to the wave function, as discussed in Sec. 1.4.

One criticism of the experiment of Lundeen *et al.* is that their method is limited to determining *pure states*, and cannot be used for *mixed states*. The distinction between these is discussed in Appendix A. Essentially, mixed states cannot be described by a wave function, but rather are described by either a density matrix or a quasiprobability distribution. This criticism was dealt with by Lundeen *et al.* in a follow-up paper [54]. It turns out that there is a quasiprobability distribution hidden in their measurement sequence. This is not surprising, since it *is* a joint measurement. In absence of post-selecting onto a single momentum measurement outcome p (*i.e.* also keeping $p = 0$ outcomes), the pointer shift is no longer given by the weak value. As indicated by Eq. 2.11, it is given by the *weak average* $\langle \boldsymbol{\pi}_p \boldsymbol{\pi}_x \rangle$. While the weak value is directly related to the wave function, the weak average is directly related to a quasiprobability distribution known as the Dirac distribution [25]. The only difference

between the two is that the latter is obtained by not post-selecting onto a single strong measurement outcome. In fact, in the case of the photon's transverse spatial state, it can be measured using the same apparatus as in Fig. 2.2, but by placing a camera at the focal plane of the lens instead of a pinhole. This was done experimentally in Ref. [6]. In contrast, by keeping the pinhole and thus keeping only one momentum outcome, this is equivalent to measuring a cross-section of the Dirac distribution, which gives the wave function.

The Dirac distribution can describe mixed states perfectly well. However, its relation to the more conventional object, the density matrix, is not a direct one. Instead, the density matrix can be obtained by performing a discrete Fourier transform of the Dirac distribution (see Sec. 5.4.3). Because the Fourier transform is a global transform, the experimental procedure of measuring the weak average $\langle \boldsymbol{\pi}_x \boldsymbol{\pi}_p \rangle$ is incapable of directly measuring an individual density matrix element. This is unfortunate for a number of reasons. First, it means that the direct measurement strategy does not apply to density matrices, and so there still lacks an operational meaning to individual density matrix elements. Second, the off-diagonal elements of the density matrix are known as coherences and are of particular interest in quantum physics (see Appendix A). In fact, key properties of a system such as entanglement can depend on particular off-diagonal elements. Thus, a method to directly measure coherences could be used to measure properties like entanglement without having to determine the entire state. Thirdly, the density matrix is much more widely used than quasiprobability distributions. Thus, extending the direct measurement method to density matrices would be of interest to a wider audience. Finally, direct measurement would offer a more efficient method to determine the density matrix than quantum state tomography (more details on this in Ch. 3). All these reasons motivated a way to extend direct measurement to density matrices. As it turns out, this requires us to think about weak measurements beyond two sequential measurements.

2.3.3 Extending beyond two observables

The discussion thus far has been limited to jointly measuring two observables. Here I present some key features when extending the idea to N observables, each one labeled by $\boldsymbol{A}_i$ for i from $1,...N$. In absence of post-selection, the average outcome of this measurement is given by the weak average $\langle \boldsymbol{A}_1 \boldsymbol{A}_2 ... \boldsymbol{A}_N \rangle$.

Firstly, as with strong measurements, it is important to note that for a se-

quence of N weak measurements:

$$\langle \boldsymbol{A}_1 \boldsymbol{A}_2 ... \boldsymbol{A}_N \rangle \neq \langle \boldsymbol{A}_1 \rangle \langle \boldsymbol{A}_2 \rangle ... \langle \boldsymbol{A}_N \rangle . \tag{2.14}$$

This means that jointly measuring the N properties is (in general) not equivalent to measuring each property separately and multiplying the results. This is obvious, since one expects there can be correlations between the properties (see Sec. 1.3).

Secondly, in general, the weak average $\langle \boldsymbol{A}_1 \boldsymbol{A}_2 ... \boldsymbol{A}_N \rangle$ will be complex, as was the case for $N = 2$. This is because the product of non-commuting Hermitian observables need not be Hermitian, and hence can have complex eigenvalues.

Thirdly, the reader may wonder how such a complicated weak measurement sequence can be related to pointer shifts. Luckily, there is an elegant formula that provides an answer to this question. Suppose we couple an independent pointer to each measured observable via the interaction Hamiltonian:

$$\mathscr{H}_{int} = \sum_{i=1}^{N} g \boldsymbol{A}_i \boldsymbol{p}_i \tag{2.15}$$

where $g \ll 1$ is the coupling strength, and $\boldsymbol{p}_i$ is the momentum operator of the i$^{\text{th}}$ pointer. If all the pointer states are prepared in Gaussian states (standard choice in experiments) of width σ, then Lundeen and Resch [52] showed that:

$$\langle \boldsymbol{A}_1 \boldsymbol{A}_2 ... \boldsymbol{A}_N \rangle = \left(\frac{2\sigma}{g t} \right)^N \langle \boldsymbol{a}_1 \boldsymbol{a}_2 ... \boldsymbol{a}_N \rangle , \tag{2.16}$$

where $\boldsymbol{a}_i = \boldsymbol{x}_i / 2\sigma + i\sigma \boldsymbol{p}_i / \hbar$ is the standard lowering ladder operator acting on the i$^{\text{th}}$ pointer system [4], and t is the interaction time between the pointers and the system. This equation states that the average result of a sequence of weak measurements is directly related to correlations between the position and momenta of the pointers. It is important to note that the expectation value on the left-hand-side of Eq. 2.16 is evaluated with respect to the *system* state, while the expectation value on the right-hand-side is evaluated with respect to the *pointer* state. Eq. 2.16 is elegant, but somewhat hides the difficulty of experimentally implementing a long weak measurement sequence: expanding the

[4] The fact that the ladder operator appears in Eq. 2.16 is not entirely understood, since this operator usually appears in the context of a quantum harmonic oscillator. It is probably related to the fact that a Gaussian (ground state of harmonic oscillator) pointer is used, and that the pointer shift caused by the weak measurement is small.

right-hand-side shows that there are 2^N terms to measure. Furthermore, in a typical weak measurement experiment, the system and pointer are separate degrees of freedom of a single particle, as was the case in the Stern-Gerlach experiment. This facilitates implementing the interaction between the two. However, since each observable requires its own pointer, one quickly runs out of degrees of freedom to use with this strategy.

Fourthly, the last measurement in a sequence of weak measurements can always be replaced by a strong measurement [54]. Since there are no measurements performed afterwards, the last measurement can collapse the state without affecting the outcome of the measurement sequence.

Lastly, the weak average is not invariant under re-ordering of the measurement sequence:

$$\langle \boldsymbol{A}_1 \boldsymbol{A}_2 ... \boldsymbol{A}_i ... \boldsymbol{A}_j ... \boldsymbol{A}_N \rangle \neq \langle \boldsymbol{A}_1 \boldsymbol{A}_2 ... \boldsymbol{A}_j ... \boldsymbol{A}_i ... \boldsymbol{A}_N \rangle . \tag{2.17}$$

Some work has shown that this last point can be related to quantum chaos [102] and to time-symmetry in quantum mechanics [8] quantum. Moreover, sequential weak measurements, or more generally, joint measurements of N observables, can be used to investigate the fuzzy border between discrete and continuous dynamics in quantum mechanics. For example, one paper recently demonstrated that a quasi-continuous non-demolition measurement can stroboscopically probe a system, thereby measuring its trajectory in phase-space [34]. Furthermore, sequential weak measurements are of particular interest to theorists, since any generalized measurement (*i.e.* a POVM) can be decomposed into a sequence of weak measurements [65]. This gives theorists a new tool to tackle certain analytical problems. But also, if the decomposition is known, it provides one of the few recipes to implement a general POVM experimentally.

In Ch. 3, I discuss one of the experiments I completed during my masters. This experiment was the first implementation of sequential weak measurements beyond two observables (very shortly after, another experiment [73] achieving the same was also published). The experimental apparatus is now being used by others in Prof. Lundeen's group to investigate topics related to sequential weak measurements, such as time-symmetry in quantum mechanics.

Chapter 3

Direct measurement of the density matrix of a quantum system

This chapter is based on the following publication:

G. S. Thekkadath, L. Giner, Y. Chalich, M. J. Horton, J. Banker, J. S. Lundeen, "Direct measurement of the density matrix of a quantum system", *Phys. Rev. Lett*, **117** 120401 (2016) © American Physical Society.

The paper was selected as an Editor's suggestion and highlighted in the American Physical Society's *Physics* as a Viewpoint article written by Andrew N. Jordan (see Ref. [43]).

3.1 Introduction

Shortly after the inception of the quantum state, Pauli questioned its measurability, and in particular, whether or not a wave function can be obtained from position and momentum measurements [71]. This question, now referred to as the Pauli problem, draws on concepts such as complementarity and measurement in an attempt to demystify the physical significance of the quantum state. Indeed, the task of determining a quantum state is a central issue in quantum physics due to both its foundational and practical implications. For instance, a method to verify the production of complicated states is desirable in quantum information and quantum metrology applications. Moreover, since a state fully characterizes a system, any possible measurement outcome can be predicted

once the state is determined.

A wave function describes a quantum system that can be isolated from its environment, meaning the two are non-interacting and the system is in a pure state. More generally, open quantum systems can interact with their environment and the two can become entangled. In such cases, or even in the presence of classical noise, the system is in a statistical mixture of states (*i.e.* mixed state), and one requires a density matrix to fully describe the quantum system. In fact, some regard the density matrix as more fundamental than the wave function because of its generality and its relationship to classical measurement theory [36].

The standard way of measuring the density matrix is by using quantum state tomography (QST). In QST, one performs an often overcomplete set of measurements in incompatible bases on identically prepared copies of the state. Then, one fits a candidate state to the measurement results with the help of a reconstruction algorithm [1]. Many efforts have been made to optimize QST [99, 76, 29, 9], but the scalability of the experimental apparatus and the complexity of the reconstruction algorithm renders the task increasingly difficult for large dimensional systems. In addition, since QST requires a global reconstruction, it does not provide direct access to coherences (*i.e.* off-diagonal elements), which are of particular interest in quantum physics.

Some recent work has focused on developing a direct approach to measuring quantum states [55, 54, 6, 82, 60, 58, 31, 24, 100, 10, 86, 94]. Defining features of direct methods are that they can determine the state without complicated computations, and they can do so locally, *i.e.* at the location of the measurement probe. For example, direct measurement of the wave function has been achieved by performing a sequence consisting of a weak and strong measurement of complementary variables (*e.g.* position and momentum) [55]. In the sub-ensemble of trials for which the strong measurement results in a particular outcome (i.e. “post-selection"), the average weak measurement outcome is a complex number known as the weak value [3, 4]. The weak value is a concept that has proven to be useful in addressing fundamental questions in quantum physics [77, 53, 101, 68, 33, 27, 91, 48, 97, 73], even beyond optics [87]. By foregoing post-selection, previous work [6, 82] generalized the direct wave function measurement scheme to measure mixed quantum states. However, their method still does not provide direct access to individual density matrix

[1] Some reconstruction algorithms restrictively fit the measurement results to reconstruct only physical (*i.e.* positive semi-definite and normalized) states.

elements. Ref. [54] proposes a way to do this by performing an additional complementary measurement after the wave function measurement sequence: The second measurement serves as a phase reference and enables the first and last measurements to probe the coherence between any two chosen states in some basis. On top of its applications, a direct measurement method provides an operational meaning to the density matrix in terms of a sequence of three complementary measurements.

3.2 Theory

We experimentally demonstrate the method proposed in Ref. [54] by directly measuring any chosen element of a density matrix $\boldsymbol{\rho}_S$ of a system S. By repeating this for each element, we then measure the entire density matrix, thereby completely determining the state of the system. At the center of the method is a sequence of incompatible measurements [72, 92]. In order for these measurements not to disrupt each other, they are made weak, a concept that we outline now (for a review, see [28]). Suppose one wishes to measure the observable $\boldsymbol{C}$. In von Neumann's model of measurement, the measured system S is coupled to a separate "pointer" system P whose wave function is initially centered at some position and has a width σ. This coupling proportionally shifts the position of the pointer by the value of $\boldsymbol{C}$ as described by the unitary translation $\boldsymbol{U} = \exp(-i\delta\boldsymbol{C}\boldsymbol{p}/\hbar)$, where $\boldsymbol{p}$ is the pointer momentum operator and δ is strength of the interaction. After the coupling, the pointer position q is measured. On a trial by trial basis, if $\delta \gg \sigma$, the pointer position will be shifted by $\Delta q \approx \delta c$ and thus will indicate that the result of the measurement of $\boldsymbol{C}$ is c.

In contrast, in weak measurement $\delta \ll \sigma$, and the measurement result is ambiguous since it falls within the original position distribution of the pointer. However, this does have a benefit: The small interaction leaves the measured system relatively undisturbed and thus it can subsequently be measured again [41]. By repeating the weak measurement on an ensemble of systems and averaging, the shift of the pointer can be found unambiguously. This average shift is called the "weak average" $\langle \boldsymbol{C} \rangle_S$ and is equal to the expectation value of a conventional (*i.e.* "strong") measurement: $\langle \boldsymbol{C} \rangle_S = \mathrm{Tr}_S[\boldsymbol{C}\boldsymbol{\rho}_S]$ [54]. This differs from the weak value normally encountered in that there is no post-selection.

Unlike in strong measurement, $\boldsymbol{C}$ can be non-Hermitian. This is the case when $\boldsymbol{C}$ is the product of incompatible observables which normally disturb each other. Consequently, it is possible for the weak average to be complex.

What does this imply? Both the position $\boldsymbol{q}$ and momentum $\boldsymbol{p}$ of the pointer will be shifted according to $\langle \boldsymbol{C} \rangle_S = \frac{1}{\delta} \langle \mathrm{a} \rangle_P$, where $\mathrm{a} = \boldsymbol{q} + i2\sigma^2 \boldsymbol{p}/\hbar$ is the standard harmonic oscillator lowering operator scaled by 2σ [52]. The real part and imaginary parts of the weak average are proportional to the average shift of the pointer's position and momentum, respectively.

Consider the weak measurement of an observable composed of the following three incompatible projectors:

$$\boldsymbol{\Pi}_{a_i a_j} = \boldsymbol{\pi}_{a_j} \boldsymbol{\pi}_{b_0} \boldsymbol{\pi}_{a_i}, \tag{3.1}$$

where $\boldsymbol{\pi}_{a_i} = |a_i\rangle\langle a_i|$ and $\boldsymbol{\pi}_{b_0} = |b_0\rangle\langle b_0|$, which are composed of eigenstates of the observables $\boldsymbol{A}$ and $\boldsymbol{B}$, respectively. These are maximally incompatible, or "complementary", in the sense that $|\langle a_i|b_0\rangle| = 1/\sqrt{d}$ for a d-dimensional Hilbert space. In the basis of the eigenstates of $\boldsymbol{A}$, a density matrix element is given by $\rho_S(i,j) = \langle a_i|\boldsymbol{\rho}_S|a_j\rangle$. This can be connected to the weak average of the measurement sequence in Eq. 3.1:

$$\langle \boldsymbol{\Pi}_{a_i a_j} \rangle_S = \mathrm{Tr}_S \left[\boldsymbol{\pi}_{a_j} \boldsymbol{\pi}_{b_0} \boldsymbol{\pi}_{a_i} \boldsymbol{\rho}_S \right] = \rho_S(i,j)/d. \tag{3.2}$$

In fact, one can replace the weak measurement of the last projector $\boldsymbol{\pi}_{a_j}$ by a strong measurement without affecting the weak average [54], thereby reducing the complexity of the measurement apparatus. Thus any density matrix element can be obtained by selecting the first and last projectors in the measurement sequence. Whichever state $|b_0\rangle$ that is chosen for the middle complementary projector serves as a reference for zero phase in the density matrix by fixing $\theta = 0$ for all a in $\langle a|b_0\rangle = \exp(i\theta)/\sqrt{d}$. As such, it should remain fixed.

3.3 Experimental setup

The experimental setup is shown in Fig. 3.1. We demonstrate the technique by directly measuring the density matrix of a photon polarization state. This is possibly the simplest system for a demonstration, but it is also an important one since it can act as a qubit from which larger and more complicated quantum states can be constructed, such as in quantum computing. A HeNe laser at 633 nm is sent through a polarizing beam splitter (PBS) to ensure it is polarized. We treat the bright polarized beam as a source of a large number of identically prepared polarized photons. Instead of using a separate system, we use the x and y transverse spatial distributions of the photons as pointers. Both

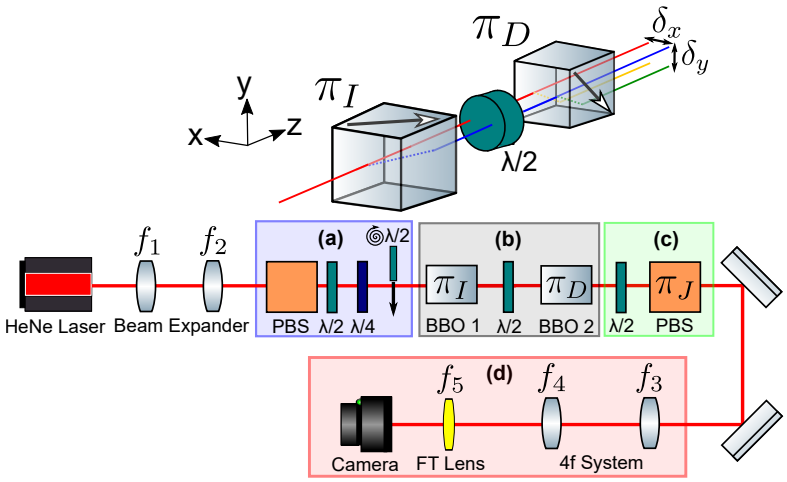

Figure 3.1: Direct measurement experimental setup. **(a)** *State preparation*: We use a HeNe laser as a source of photons. The photon polarization state is set using a half-wave plate ($\lambda/2$) and a quarter-wave plate ($\lambda/4$). A spinning $\lambda/2$ is included when generating mixed states. **(b)** *Weak measurements*: Two subsequent weak measurements $\boldsymbol{\pi}_I$ and $\boldsymbol{\pi}_D$ are performed, each with a walk-off crystal (BBO) that couples the polarization to a spatial degree of freedom, x or y, our measurement pointers. Note that $\delta_x = \delta_y \equiv \delta$. **(c)** *Strong measurement*: The final measurement $\boldsymbol{\pi}_J$ is performed by a polarizing beam splitter (PBS), and the projection direction J is set by a $\lambda/2$. **(d)** *Imaging*: A 4f arrangement of lenses forms an image of the crystal plane onto a camera allowing us to measure pointer positions. An additional Fourier transform (FT) lens, either spherical or cylindrical, is used to measure pointer momenta.

are Gaussian with widths $\sigma = 250$ μm (830 μm FWHM) that are set using a telescopic arrangement of two convex lenses ($f_1 = 50$ mm and $f_2 = 100$ mm). We set the photon polarization state $\boldsymbol{\rho}_S$ using a half-wave plate ($\lambda/2$) and a quarter-wave plate ($\lambda/4$).

A weak measurement of polarization is implemented by coupling the polarization degree of freedom (our system) to a spatial one (a pointer). This is accomplished with a walk-off crystal (beta barium borate, BBO) that shifts the $|I\rangle$ polarization component along x by $\delta = 176$ μm. If $\delta \gg \sigma$ this implements a strong measurement of $\boldsymbol{\pi}_I = |I\rangle\langle I|$ since the photon position unambiguously determines $\boldsymbol{\pi}_I$. If $\delta \ll \sigma$ this is a weak measurement of $\boldsymbol{\pi}_I$ [2]. In our demonstration, we find each of the four polarization density matrix elements $\rho_S(I,J)$ by measuring the three projector observable $\boldsymbol{\pi}_J\boldsymbol{\pi}_D\boldsymbol{\pi}_I$ where either I or J can be horizontal H or vertical V polarization and $|D\rangle = (|H\rangle + |V\rangle)/\sqrt{2}$ is a complementary state, the diagonal polarization.

Coupling a joint observable $\boldsymbol{EF}$ such as $\boldsymbol{\pi}_D\boldsymbol{\pi}_I$ to a single pointer is challenging for photons. Instead, we follow a strategy commonly used for joint strong measurements (*e.g.* those in Bell's inequalities) in which one independently measures single observables and then evaluates correlations between the independent results. In von Neumann's model, this corresponds to having two independent pointers so that $\langle \boldsymbol{EF}\rangle_S = \left(\frac{1}{\delta}\right)^2 \langle \boldsymbol{q}_E \boldsymbol{q}_F\rangle_P$, where $\boldsymbol{q}_m$ is the position of the $m = E, F$ pointer. In the weak measurement analog, proposed in Ref. [52], one replaces $\boldsymbol{q}_m$ by a_m, and so $\langle \boldsymbol{EF}\rangle_S = \left(\frac{1}{\delta}\right)^2 \langle \mathrm{a}_E \mathrm{a}_F\rangle_P$ [61, 54]. Thus we can couple $\boldsymbol{\pi}_I$ and $\boldsymbol{\pi}_D$ to separate pointers and then measure correlations between the momenta and positions of these pointers to find the weak average. The final measurement in the sequence $\boldsymbol{\pi}_J$ is strong and so the full joint expectation value is

$$\langle \boldsymbol{\Pi}_{IJ}\rangle_S = \left(\frac{1}{\delta}\right)^2 \mathrm{Tr}_T[\boldsymbol{\pi}_J \mathrm{a}_D \mathrm{a}_I \boldsymbol{\rho}_T] = \rho_S(I,J)/2, \tag{3.3}$$

where $T = S \otimes P$ indicates the total Hilbert space, combining the pointers and the system ($d = 2$).

In our experiment, we conduct two independent weak measurements by sequentially introducing two walk-off crystals in the beam path (see Sec. 3.6 for alignment procedure). The first measures $\boldsymbol{\pi}_I$ by inducing a displacement δ along x. Combined with a $\lambda/2$ at 22.5°, the second crystal induces a displacement δ along y, measuring $\boldsymbol{\pi}_D$. The last projector $\boldsymbol{\pi}_J$, the strong measurement,

[2] A walk-off crystal is used for weak measurement of polarization in, for example, Refs. [82, 79]

is implemented by a second $\lambda/2$ and a PBS where the $\lambda/2$ is used to choose the projected state $J = H, V$, *i.e.* a J polarizer.

The lowering operators in the total pointer-system expectation value in Eq. 3.3 imply the measurement of positions and momenta of the photons. Experimentally, we measure quantities such as the probability that a photon is transmitted through the final J polarizer, and also has horizontal position x and vertical position y, *i.e.* Prob(x, y, J) [3]. From this, we can find expectation values such as $\iint xy\text{Prob}(x, y, J)dxdy \equiv \langle \boldsymbol{xy} \rangle_{P,J}$ (see Sec. 3.6 for an example). Then the density matrix elements can be directly related to the joint position $(\boldsymbol{x}, \boldsymbol{y})$ and momentum $(\boldsymbol{p}_x, \boldsymbol{p}_y)$ expectation values of the pointer state:

$$\begin{aligned} \text{Re}[\rho_S(I,J)] &= \frac{2}{\delta^2}\left(\langle \boldsymbol{x}_I \boldsymbol{y}_D \rangle_{P,J} - \frac{\sigma^2}{\sigma_p^2}\langle \boldsymbol{p}_{xI} \boldsymbol{p}_{yD} \rangle_{P,J}\right), \\ \text{Im}[\rho_S(I,J)] &= \frac{2}{\delta^2}\frac{\sigma}{\sigma_p}\left(\langle \boldsymbol{p}_{xI} \boldsymbol{y}_D \rangle_{P,J} + \langle \boldsymbol{x}_I \boldsymbol{p}_{yD} \rangle_{P,J}\right). \end{aligned} \tag{3.4}$$

Eq. 3.4 is expressed using σ and σ_p where $\sigma\sigma_p = \hbar/2$ to explicitly remove the unit dependence of position and momentum. The subscript I in *e.g.* $\langle \boldsymbol{x}_I \boldsymbol{y}_D \rangle$ indicates the projector $\boldsymbol{\pi}_I$ is coupled to the $\boldsymbol{x}$ pointer.

We measure the four joint expectation values in Eq. 3.4 one at a time using a camera (CMOS sensor with resolution 2560x1920 and pixel side length of 2.2 μm). The position expectation value $\langle \boldsymbol{xy} \rangle$ of the pointer state is obtained using two convex lenses (f_3 = 1000 mm and f_4 = 1200 mm) in a 4f arrangement that images the crystal plane onto the camera. The momentum expectation value $\langle \boldsymbol{p}_x \boldsymbol{p}_y \rangle$ is obtained by adding a spherical lens (f_5 = 1000 mm) one focal length from the camera. We replace the spherical lens with a cylindrical one (also f_5) to take a one-dimensional Fourier transform of the pointer states and measure the expectation values $\langle \boldsymbol{p}_x \boldsymbol{y} \rangle$ and $\langle \boldsymbol{p}_y \boldsymbol{x} \rangle$ by rotating the axis cylindrical lens. In order to obtain each and every density matrix element, we repeat these four measurements for all combinations of (I, J).

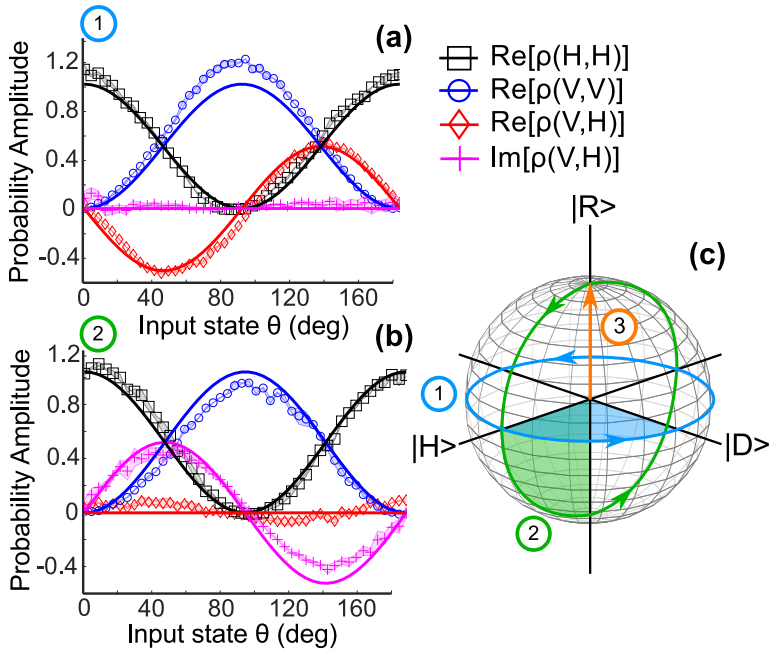

Figure 3.2: Direct measurement of density matrix elements for pure polarization states. **(a)** and **(b)** are the density matrix elements along path 1 and 2 in the Poincaré sphere, respectively. The bold lines are the theoretical matrix elements given by Eq. 3.5, while the markers are data points. The shaded region in these plots represents one standard deviation from averaging over ten trials, and is mostly smaller than the size of the markers. **(c)** Poincaré sphere. Path 3 corresponds to the measurement of mixed states, shown in Fig. 3.3. The shaded regions indicate an interval of $\Delta\theta = 45°$ to help the reader link the paths to the θ axes in (a) and (b).

3.4 Results

First, we measure the density matrix elements of the pure state $|\psi\rangle = \cos\theta\,|H\rangle - \sin\theta e^{i\alpha\pi/2}\,|V\rangle$:

$$\boldsymbol{\rho} = |\psi\rangle\langle\psi| = \begin{pmatrix} \cos^2\theta & -e^{-i\alpha\pi/2}\cos\theta\sin\theta \\ -e^{i\alpha\pi/2}\cos\theta\sin\theta & \sin^2\theta \end{pmatrix}. \tag{3.5}$$

Fig. 3.2a shows density matrix elements along path 1 in the Poincare sphere, which is traced by setting $\alpha = 0$ (*i.e.* removing the $\lambda/4$) and varying the fast-axis of the $\lambda/2$ such that $\theta \in [0, 180°]$. Fig. 3.2b shows the same density matrix elements along path 2, which is by traced by setting $\alpha = -1$ (*i.e.* $\lambda/4$ fast axis at $-\pi/2$) and again varying the fast-axis of the $\lambda/2$ such that $\theta \in [0, 180°]$. As can be seen, the measured density matrix elements closely follow the theory curve. Deviations from the curve (*e.g.* near $\theta = 90°$) are likely due to imperfections in the wave plates, which can introduce systematic errors both when preparing the polarization state and aligning the BBO crystals.

Next, we generate mixed states by creating a incoherent combination of pure states. This is achieved by introducing a spinning $\lambda/2$ in the preparation stage. This $\lambda/2$ rotates sufficiently fast such that over the exposure time of the camera, the measured result contains contributions from many polarization states (see Sec. 3.6). In particular, we produce

$$\boldsymbol{\rho} = \begin{pmatrix} 1/2 & i\sin\phi\cos\phi \\ -i\sin\phi\cos\phi & 1/2 \end{pmatrix}, \tag{3.6}$$

where ϕ is the angle between horizontal and the fast axis of the $\lambda/4$. We generate a series of such mixed states (see Fig. 3.3b) and vary their purity $\mathrm{Tr}[\boldsymbol{\rho}^2]$ between 1/2 and 1 by adjusting ϕ. This corresponds to path 3 in the Poincaré sphere, as shown in Fig. 3.2c. To measure the accuracy of our measured density matrices, we compute the trace distance $\left|\mathrm{Tr}\left[\sqrt{(\boldsymbol{\beta}-\boldsymbol{\rho})^\dagger(\boldsymbol{\beta}-\boldsymbol{\rho})}\right]\right|/2$ ($\boldsymbol{\beta}$ is the measured state) which is shown in Fig. 3.3c. The trace distance can be interpreted as a measure of the maximum probability of distinguishing between two states, $\boldsymbol{\rho}$ and $\boldsymbol{\beta}$, with an optimal measurement. For our results, this probability is always less than 4.9 %. We also note that the measured density matrix

[3] We note that this is not the same as a post-selection since we do not re-normalize the state after passing through the J polarizer, *i.e.* the probability is not conditional on $\boldsymbol{\pi}_J$. Prob(x, y, J) is one value of the total normalized probability distribution.

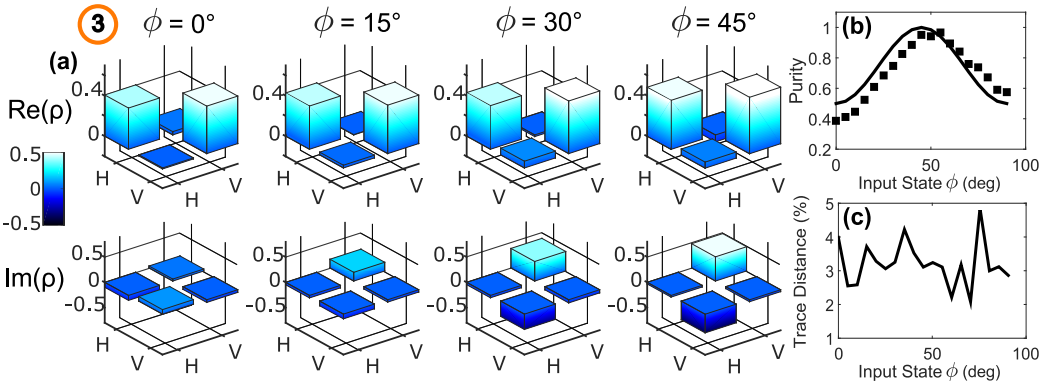

Figure 3.3: Direct measurement of mixed states. **(a)** Measured density matrices. The color is proportional to the measured probability amplitudes. **(b)** States with various degrees of purity $\mathrm{Tr}[\boldsymbol{\rho}^2]$ can be generated by varying the fast axis angle ϕ of a $\lambda/4$, as shown in Eq. 3.6. The bold line is the theory while the markers are data points. The states follow path 3 in the Poincaré sphere shown in Fig. 3.2. We do not show statistical uncertainties as they are smaller than the markers. **(c)** The trace distance is half the Euclidean distance between the measured and theory states on the Poincaré sphere, and is always less than 0.049 (*i.e.* 4.9 %).

may not be positive semi-definite due to measurement uncertainties. Consequently, if one requires a positive semi-definite matrix, one would need to employ additional algorithms such as a maximum-likelihood estimation.

3.5 Conclusion

To summarize, we directly measure the density matrix elements of photons in both pure and mixed polarization states using three sequential measurements, each complementary to the last. The first two measurements are weak to minimize their disturbance on the state, while the last measurement is strong. The average joint result of this measurement sequence gives any chosen density matrix element, and hence, can be used to operationally define the density matrix.

We anticipate that this method will be of use in practical applications. Since the last measurement can be weak, it could function as a non-invasive probe to determine a quantum state *in situ*, such as during a quantum computation or molecular evolution. Moreover, one could envisage directly observing global properties of a state, such as the existence of non-classical correlations [92], by measuring coherences or entanglement witnesses with our method. Lastly, direct measurement has already proven to be efficient for measuring large dimensional pure states in various physical systems [58, 10, 86]. Quantum state tomography typically requires $\mathcal{O}(d^2)$ measurements in $\mathcal{O}(d)$ bases and finds the full density matrix at once. Thus as d increases, the experimental procedure and reconstruction algorithm become increasingly complicated. In contrast, our direct measurement method requires three measurements in only two bases to determine any chosen density matrix element regardless of the system dimension d. Consequently, in systems with large d the method is an attractive alternative to tomography as a way to locally characterize a potentially mixed quantum state.

3.6 Supplementary Material

3.6.1 Example of pointer state expectation value

Here we give an example of a pointer state expectation value for the specific case of $(I,J) = (H,H)$. In this case, the measurement sequence is $\boldsymbol{\pi}_H \boldsymbol{\pi}_D \boldsymbol{\pi}_H$

where *e.g.* $\boldsymbol{\pi}_H = |H\rangle\langle H|$. We assume that the polarization state is pure for simplicity.

The total state $|\Psi\rangle \in H_T$ describing the photons before the measurement is the product state of their spatial $|\chi\rangle \in H_P$ and polarization $|\psi\rangle \in H_S$ degrees of freedom:

$$|\Psi\rangle = |\chi\rangle \otimes |\psi\rangle = |\chi\rangle \otimes (a|H\rangle + b|V\rangle)\,. \tag{3.7}$$

The spatial degree of freedom is used as a pointer state $|\chi\rangle = |\chi_x\rangle \otimes |\chi_y\rangle$ and is determined by the Gaussian intensity profile of the HeNe laser, namely

$$\langle\zeta|\chi_\zeta\rangle \equiv \chi_\zeta(\zeta) = \left(\frac{1}{\sqrt{2\pi}\sigma_\zeta}\right)^{1/2} e^{-\frac{\zeta^2}{4\sigma_\zeta^2}} \tag{3.8}$$

for $\zeta \to \{x, y\}$. We assume the pointers are centered at zero before any interaction with the birefringent crystals.

The first walk-off crystal implements the weak projector $\boldsymbol{\pi}_H$, and hence the x pointer state $|\chi_x\rangle$ associated with the $|H\rangle$ polarization state is shifted by δ_x, which we describe as some unitary transformation $\boldsymbol{U}_1$:

$$\langle\vec{r}|\boldsymbol{U}_1|\Psi\rangle = a\chi_x(x-\delta_x)\chi_y(y)\,|H\rangle + b\chi_x(x)\chi_y(y)\,|V\rangle \tag{3.9}$$

where $\vec{r} = (x, y)$. We can express the result above in the diagonal basis using $|H\rangle = (|D\rangle - |A\rangle)/\sqrt{2}$ and $|V\rangle = (|D\rangle + |A\rangle)/\sqrt{2}$:

$$\begin{aligned}\langle\vec{r}|\boldsymbol{U}_1|\Psi\rangle = &\left(\frac{a}{\sqrt{2}}\chi_x(x-\delta_x)\chi_y(y) + \frac{b}{\sqrt{2}}\chi_x(x)\chi_y(y)\right)|D\rangle \\ &-\left(\frac{a}{\sqrt{2}}\chi_x(x-\delta_x)\chi_y(y) - \frac{b}{\sqrt{2}}\chi_x(x)\chi_y(y)\right)|A\rangle\end{aligned} \tag{3.10}$$

Next in the measurement sequence, the second walk-off crystal implements $\boldsymbol{\pi}_D$. The y pointer state $|\chi_y\rangle$ associated with the $|D\rangle$ polarization is shifted by δ_y, which we describe by $\boldsymbol{U}_2$:

$$\begin{aligned}\langle\vec{r}|\boldsymbol{U}_2\boldsymbol{U}_1|\Psi\rangle = &\left(\frac{a}{\sqrt{2}}\chi_x(x-\delta_x)\chi_y(y-\delta_y) + \frac{b}{\sqrt{2}}\chi_x(x)\chi_y(y-\delta_y)\right)|D\rangle \\ &-\left(\frac{a}{\sqrt{2}}\chi_x(x-\delta_x)\chi_y(y) - \frac{b}{\sqrt{2}}\chi_x(x)\chi_y(y)\right)|A\rangle\end{aligned} \tag{3.11}$$

Finally, the last measurement $\boldsymbol{\pi}_H$ is strong. It is implemented by a polarizing beam splitter (PBS) with transmits only $|H\rangle$ to the camera. After the PBS, the

total state is given by:

$$\begin{aligned}\langle \vec{r}|\boldsymbol{\pi}_H \boldsymbol{U}_2 \boldsymbol{U}_1|\Psi\rangle = \frac{a}{2}\left(\chi_x(x-\delta_x)\chi_y(y-\delta_y)+\chi_x(x-\delta_x)\chi_y(y)\right)|H\rangle \\ + \frac{b}{2}\left(\chi_x(x)\chi_y(y-\delta_y)-\chi_x(x)\chi_y(y)\right)|H\rangle\,.\end{aligned} \tag{3.12}$$

Thus by measuring the final state of the pointers, the camera records the probability Prob(x, y, H) that a photon has a position (x, y) *and* polarization $|H\rangle$:

$$\begin{aligned}\text{Prob}(x,y,H) = \Big|\frac{a}{2}\left(\chi_x(x-\delta_x)\chi_y(y-\delta_y)+\chi_x(x-\delta_x)\chi_y(y)\right) \\ + \frac{b}{2}\left(\chi_x(x)\chi_y(y-\delta_y)-\chi_x(x)\chi_y(y)\right)\Big|^2.\end{aligned} \tag{3.13}$$

We can now compute the various expectation values required. For instance:

$$\begin{aligned}\langle \boldsymbol{x}_H \boldsymbol{y}_D\rangle_{P,H} &= \int_{-\infty}^{\infty}\int_{-\infty}^{\infty} xy\,\text{Prob}(x,y,H)\,dx\,dy \\ &= \frac{|a|^2}{4}\delta_x\delta_y(1+e^{\frac{-\delta_y^2}{8\sigma_y^2}}) + \frac{1}{4}\frac{(ab^*+a^*b)}{2}(\delta_x\delta_y e^{\frac{-\delta_x^2}{8\sigma_x^2}})\end{aligned} \tag{3.14}$$

which in the weak measurement limit ($\delta_x \ll \sigma_x$ and $\delta_y \ll \sigma_y$) reduces to

$$\langle \boldsymbol{x}_H \boldsymbol{y}_D\rangle_{P,H} = \frac{\delta_x\delta_y}{4}\left(2|a|^2 + \frac{ab^*+a^*b}{2}\right). \tag{3.15}$$

To be clear, the first subscript H in $\langle \boldsymbol{x}_H \boldsymbol{y}_D\rangle_{P,H}$ indicates that the first weak measurement $\boldsymbol{\pi}_H$ is coupled to the $\boldsymbol{x}$ pointer, while the second H subscript indicates that the last strong measurement is $\boldsymbol{\pi}_H$. If we repeat similar calculations for the other required expectation values (and take the Fourier transform where required), we obtain

$$\begin{aligned}\langle \boldsymbol{p}_{xH}\boldsymbol{p}_{yD}\rangle_{P,H} &= \frac{\delta_x\delta_y}{16\sigma_x^2\sigma_y^2}\left(\frac{ab^*+a^*b}{2}\right) \\ \langle \boldsymbol{p}_{xH}\boldsymbol{y}_D\rangle_{P,H} &= \frac{\delta_x\delta_y}{8\sigma_x^2}\left(\frac{iab^*-ia^*b}{2}\right) \\ \langle \boldsymbol{p}_{yH}\boldsymbol{x}_D\rangle_{P,H} &= \frac{\delta_x\delta_y}{8\sigma_y^2}\left(\frac{-iab^*+ia^*b}{2}\right).\end{aligned} \tag{3.16}$$

For our crystals, the pointer shifts are the same $\delta_x = \delta_y = \delta$, as well as the pointer widths $\sigma_x = \sigma_y = \sigma$. We can introduce the momentum space width σ_p

of the pointer state by noting that $\sigma\sigma_p = 1/2$ (see Eq. 3.8). With these changes, we find that:

$$\begin{aligned} \mathrm{Re}[\rho(H,H)] &= \frac{2}{\delta^2}\left(\langle \boldsymbol{x}_H \boldsymbol{y}_D\rangle_{P,H} - \frac{\sigma^2}{\sigma_p^2}\langle \boldsymbol{p}_{xH}\boldsymbol{p}_{yD}\rangle_{P,H}\right) = |a|^2, \\ \mathrm{Im}[\rho(H,H)] &= \frac{2}{\delta^2}\frac{\sigma}{\sigma_p}\left(\langle \boldsymbol{p}_{xH}\boldsymbol{y}_D\rangle_{P,H} + \langle \boldsymbol{p}_{yH}\boldsymbol{x}_D\rangle_{P,H}\right) = 0. \end{aligned} \tag{3.17}$$

We note that, in the case of a two dimensional state, the expectation values in Eq. 3.16 are sufficient to obtain both parameters a and b of the state (up to a common phase), since $\mathrm{Re}(ab^*) \propto \langle \boldsymbol{p}_{xH}\boldsymbol{p}_{yD}\rangle_{\mathscr{P},H}$ and $\mathrm{Im}(ab^*) \propto \langle \boldsymbol{p}_{xH}\boldsymbol{y}_D\rangle_{P,H} - \langle \boldsymbol{p}_{yH}\boldsymbol{x}_D\rangle_{P,H}$. This implies that a single measurement sequence configuration (*e.g.* $\boldsymbol{\pi}_H\boldsymbol{\pi}_D\boldsymbol{\pi}_H$) is sufficient for measuring all parameters of the $d = 2$ state. However, for higher dimensional states, one would need to change the first and last measurements in the sequence in order to obtain an arbitrary density matrix element. For proof-of-concept, in the experiment we change the measurement sequence to obtain the various density matrix elements even in the $d = 2$ case. Other expectation values (*e.g.* $\langle \boldsymbol{x}_V \boldsymbol{y}_D\rangle_{P,H}$) are not given in this example, but can be derived with a very similar calculation.

Furthermore, we also note that the density matrix element $\rho(H,H)$ (and also $\rho(V,V)$) can be found trivially by measuring the relative intensity of the state after passing through a PBS since $\langle\psi|\boldsymbol{\pi}_H|\psi\rangle = |a|^2$. In general, the diagonals of a density matrix can be found easily by measuring projectors in the basis of the matrix. However, we do not rely on this approach in our experiment since we aim to compare our direct measurement method with conventional methods. Furthermore, as the dimension of the space becomes large, the diagonal elements will become an increasingly small fraction of the total elements that need to be determined. Thus, the benefit of switching procedures just for these diagonal elements will decrease as the dimension increases.

3.6.2 Data Acquisition Method

A camera captures 10 images for each input state. Each image is processed in the following manner. First we subtract a background image that is captured when the laser is blocked. Then we crop the image, and apply a high-frequency Fourier filter in order to further suppress noise contributions from the background and also remove fringes in the image that arise due to the camera window. Finally, we average over the 10 images to account for a random error of

Pointer state	BBO 1	BBO 2
Red	V	H
Blue	H	H
Green	H	V
Yellow	V	V

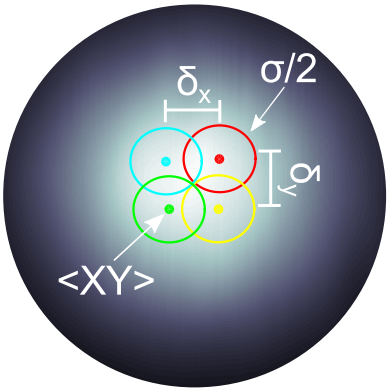

Figure 3.4: In the circle we show cropped (and superimposed) images of the four maximally shifted pointer states, after being processed. The colored circles designate the contours of the four pointer states at $\sigma/2$. The crystal shifts $\delta_x = \delta_y$ are shown for comparison. The table displays polarizations needed before each crystal to obtain the desired pointer shift.

roughly $\pm 5\%$ of the expectation values. This random error arises due to air fluctuations or small instabilities in the intensity of the laser.

The expectation values are computed with respect to the center (x_0, y_0) of the unshifted pointer state, obtained by sending $|V\rangle$-polarized photons through BBO 1 and $|H\rangle$-polarized photons through BBO 2, as shown by the red circle in Fig. 3.4. For example, the position expectation value is given by

$$\langle \boldsymbol{xy} \rangle_{P,J} = \sum_{i,j} (x_i - x_0)(y_j - y_0) \text{Prob}(x_i, y_j, J) \tag{3.18}$$

where $\text{Prob}(x, y, J)$ is a greyscale image of the pointer state with no Fourier lens, normalized to the intensity of the pointer state before any measurements. Similar equations as Eq. 3.18 are used to obtain the other joint momentum and position expectation values.

We super-impose images of the maximally shifted pointer states in Fig. 3.4 to demonstrate the size of the shifts relative to the pointer widths. The colored bold lines designate the contour of the pointer states at $\sigma/2$. The table in Fig. 3.4 provides the polarization states required before each crystal to obtain the desired pointer shift. For example, the blue pointer state is obtained when we send $|H\rangle$-polarized photons through the first BBO crystal, then $|V\rangle$-polarized photons through the second BBO crystal. This pointer state is maximally shifted in x and we can use it to obtain δ_x by computing $\delta_x = \langle \boldsymbol{x} \rangle - x_0$

where $\langle \boldsymbol{x} \rangle$ is its expectation value along x and x_0 is the center of the unshifted (red) pointer state. Similarly, the yellow pointer state is maximally shifted in y and is used to obtain δ_y. We find that $\delta_x = \delta_y = 175\ \mu m$ and the pointer width is $\sigma_x = \sigma_y = 250\ \mu$m (standard deviation as defined in Eq. 3.8, or 830 μm full-width at half-max). A cylindrical and spherical lens are used to take a Fourier transform. We find that the pointer widths in the Fourier domain are $\sigma_{p_x} = \sigma_{p_y} = 90\ \mu m$ (or 300 μm full-width at half-max).

3.6.3 Barium Borate Crystals Alignment

We use two birefringent barium borate (BBO) crystals (also referred to as walk-off crystals) to couple the spatial and polarization degrees of freedom of the photons and preform the weak measurements. To align the first BBO, we first remove the second BBO, and send $|D\rangle$-polarized photons through the experimental setup. The crystal axis is oriented to cause a spatial walk-off between the respective pointer states of the $|H\rangle$ and $|V\rangle$ components of the photons, along x. This achieves the projection $\boldsymbol{\pi}_H$. We then tilt the crystal axis along the direction of the walk-off to compensate for the different optical path length between each polarization component. To verify that we aligned properly, we set the last strong projection measurement to $\boldsymbol{\pi}_A$ in order to project onto the orthogonal polarization $|A\rangle$. We then adjust the tilt of the crystal until two faint spots displaced in x can be seen on the camera, which indicates that the pointer states of each polarization components are interfering destructively where they overlap. A very similar procedure is repeated to align BBO 2.

3.6.4 Mixed State Generation

In order to generate mixed states, we create a classical mixture of pure states by using a spinning $\lambda/2$. Given $|H\rangle\langle H|$, sending it through a $\lambda/4$ with its fast-axis at an angle ϕ will transform it $\boldsymbol{\rho} = |\psi\rangle\langle\psi|$ where $|\psi\rangle = (\cos^2\phi - i\sin^2\phi)|H\rangle + \frac{1}{2}(1+i)\sin 2\phi |V\rangle$. We subsequently send this state through a $\lambda/2$, which is described by the unitary $\boldsymbol{U} = \begin{pmatrix} \cos 2\alpha & \sin 2\alpha \\ \sin 2\alpha & -\cos 2\alpha \end{pmatrix}$ where α is the fast-axis angle of the $\lambda/2$. If the $\lambda/2$ is spinning *i.e.* $\alpha \in [0, 2\pi]$ over the exposure time of the camera, the resulting state is given by

$$\tilde{\boldsymbol{\rho}} = \frac{1}{2\pi}\int_0^{2\pi} \boldsymbol{U}\boldsymbol{\rho}\boldsymbol{U}^\dagger d\alpha = \begin{pmatrix} 1/2 & i\sin\phi\cos\phi \\ -i\sin\phi\cos\phi & 1/2 \end{pmatrix}. \tag{3.19}$$

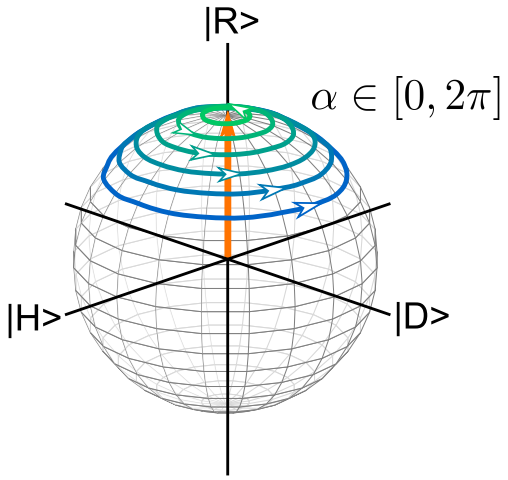

Figure 3.5: The generation of mixed states can be visualized on the Poincaré sphere. Each angle ϕ corresponds to a certain latitude on the sphere. Over the exposure time of the camera we generate a mixture of states in $\alpha \in [0, 2\pi]$ at a given latitude ϕ, and thus the resulting state lies along the $|R\rangle$ axis, as given by Eq. 3.19. In order the rotate the $\lambda/2$ sufficiently quickly over the exposure time of the camera, we mount it on a brushless motor.

Thus by varying ϕ, we can produce mixed states with a varying purity: $\mathrm{Tr}[\tilde{\boldsymbol{\rho}}^2] = 1/2 + 2(\sin\phi\cos\phi)^2$. This procedure can be visualized on the Poincaré sphere, as shown in Fig. 3.5. The camera records an image that has contributions from all the polarizations states along a latitude determined by ϕ. Averaging over these states, the resulting state $\tilde{\boldsymbol{\rho}}$ lies along the $|R\rangle$ axis, and its purity increases with its distance from the origin. The exposure time of the camera (60 ms) sets a lower bound on the angular speed of the $\lambda/2$ of roughly 13 rad/s. This is achieved by mounting the wave plate on a brushless gimbal motor.

Chapter 4

Quantum cloning

In the previous chapters, we examined in detail a type of measurement that minimizes its disturbance to the system being measured. We saw that non-commuting properties can be jointly measured by performing these weak measurements sequentially, as in Ch. 3.

Another naive strategy that one may consider to perform a joint measurement is to first copy the system being measured, and measure each property on a separate copy. In that way, although the measurements collapse the state, since these are not performed on the same copy sequentially, they no longer disrupt each other. There are two major issues with this strategy: the no-cloning theorem and the fact that the measurement results from separate copies are not correlated. The importance of these correlations was discussed in Sec. 1.3. Instead, I focus on the no-cloning theorem below. Afterwards, I introduce some key concepts related to cloning in quantum mechanics that will help the reader better understand the experiment in Ch. 5.

4.1 No-cloning theorem

The no-cloning theorem states that it is impossible to make a perfect copy of an arbitrary quantum state. In other words, it states that quantum information cannot be copied. It was proven by Wootters and Zurek in 1982 [98]. The fact that the theorem was proven long after the inception of quantum mechanics is remarkable given its fundamental importance and the simplicity of the proof (see below). Indeed, no-cloning is a key feature of quantum physics, since classically, copying is a common occurrence (*e.g.* DNA replication or amplifica-

tion). It now plays a vital role in many areas of quantum physics. For instance, it is the bedrock of the security of quantum cryptography, since it implies that an eavesdropper cannot tap a secure quantum channel without being detected. It is also being used to understand the faith of information during the evaporation of black holes to maybe solve the famous black hole information paradox [2].

The proof of the no-cloning only assumes that quantum mechanics is a linear theory. This assumption is, of course, valid, since transformations in quantum mechanics are described by linear operators, *e.g.* $\boldsymbol{A}$, that must satisfy:

$$\boldsymbol{A}\left(\lambda_1 |\psi\rangle + \lambda_2 |\phi\rangle\right) = \lambda_1 \boldsymbol{A}|\psi\rangle + \lambda_2 \boldsymbol{A}|\phi\rangle\,. \tag{4.1}$$

where λ_1 and λ_2 are complex numbers, and $|\psi\rangle$ and $|\phi\rangle$ are normalized states. Now to prove the theorem. Suppose we had one such linear transformation $\boldsymbol{A}$ that created a copy of an arbitrary state:

$$|\psi\rangle \otimes |0\rangle \xrightarrow{\boldsymbol{A}} |\psi\rangle \otimes |\psi\rangle\,. \tag{4.2}$$

Similarly, we should also be able to copy another state $|\phi\rangle$:

$$|\phi\rangle \otimes |0\rangle \xrightarrow{\boldsymbol{A}} |\phi\rangle \otimes |\phi\rangle\,. \tag{4.3}$$

Now suppose we want to copy a superposition of these states: $(|\psi\rangle + |\phi\rangle)/\sqrt{2}$. By linearity and using Eq. 4.2 and Eq. 4.3, we find:

$$\frac{|\psi\rangle + |\phi\rangle}{\sqrt{2}} \otimes |0\rangle = \frac{|\psi\rangle \otimes |0\rangle}{\sqrt{2}} + \frac{|\phi\rangle \otimes |0\rangle}{\sqrt{2}} \xrightarrow{\boldsymbol{A}} \frac{|\psi\rangle \otimes |\psi\rangle}{\sqrt{2}} + \frac{|\phi\rangle \otimes |\phi\rangle}{\sqrt{2}}. \tag{4.4}$$

Contrast this to the desired result of a copying operation:

$$\frac{|\psi\rangle + |\phi\rangle}{\sqrt{2}} \otimes |0\rangle \xrightarrow{\boldsymbol{A}} \frac{|\psi\rangle + |\phi\rangle}{\sqrt{2}} \otimes \frac{|\psi\rangle + |\phi\rangle}{\sqrt{2}}. \tag{4.5}$$

Since Eq. 4.4 and Eq. 4.5 are different, we conclude that there exists no such transformation $\boldsymbol{A}$. This is the end of the proof. By invoking the unitarity (preservation of norm) of quantum mechanics, it can be shown in a similar manner that only states satisfying $\langle\phi|\psi\rangle = \left|\langle\phi|\psi\rangle\right|^2$ (*e.g.* orthogonal states) could in principle be perfectly copied for a given $\boldsymbol{A}$. This could readily be achieved for polarization qubits with a polarizing beam splitter, for example.

4.2 Quantum cloning machines

The no-cloning theorem instigated work on quantum cloning machines (QCMs), which are transformations that can produce imperfect copies, henceforth *clones*. Here I focus on a $1 \rightarrow 2$ QCM which produces two clones of an arbitrary input state. Specifically, it takes as an input the state which one wants to copy, $|\psi\rangle$, along with a "blank piece of paper" state known as an ancilla $\boldsymbol{a}$ (which can be a mixed state). The QCM then outputs two clones of $|\psi\rangle$, labeled by $\boldsymbol{\rho}_{\psi}^{(i)}$ (they need not be pure), into separate modes. In general, the clones can emerge as an entangled state $\boldsymbol{\rho}_{\psi}^{(12)}$. Mathematically, this is written as $|\psi\rangle\langle\psi| \otimes \boldsymbol{a} \rightarrow \boldsymbol{\rho}_{\psi}^{(12)}$, where $\boldsymbol{\rho}_{\psi}^{(1)} = \mathrm{Tr}_2(\boldsymbol{\rho}_{\psi}^{(12)})$ and $\boldsymbol{\rho}_{\psi}^{(2)} = \mathrm{Tr}_1(\boldsymbol{\rho}_{\psi}^{(12)})$.

There are a vast variety of different QCMs, each with their own advantages and disadvantages, that are tailored for their specific application [83]. However, there are a few properties that are desirable for any QCM to have. These are listed here:

1. Symmetric: The clones are indistinguishable from one another, *i.e.* $\boldsymbol{\rho}_{\psi}^{(1)} = \boldsymbol{\rho}_{\psi}^{(2)}$.

2. Optimal: The QCM produces the best possible clones as theoretically possible, in terms of *fidelity* (see Appendix B) of each clone with the input state.

3. Universal: The fidelity of the clones is the same regardless of the state being copied.

In 1996, Buzek and Hillery developed a $1 \rightarrow 2$ QCM that achieves all three properties [15]. Their QCM is made universal by choosing an ancilla in a completely mixed state, $\boldsymbol{a} = \boldsymbol{I}/d$ where $\boldsymbol{I}$ is the identity operator and d the dimension of the state being cloned. This ancilla has the same overlap with any pure state, *i.e.* $\langle\psi|\boldsymbol{a}|\psi\rangle$ is the same regardless of $|\psi\rangle$. As such, $\boldsymbol{a}$ truly acts like a "blank piece of paper" with no bias towards any particular state. Moreover, the Buzek and Hillery QCM is symmetric since their cloning operation is simply a projection onto the symmetric subspace of the cloner input $|\psi\rangle\langle\psi| \otimes \boldsymbol{a}$ [1]. It was later proven that this strategy is optimal for a universal cloner, regardless of the dimension of the state [32]. For the case of polarization qubits, their cloner has

[1] Two-particle symmetric states are those that remain unchanged under particle exchange, such as the triplet spin states.

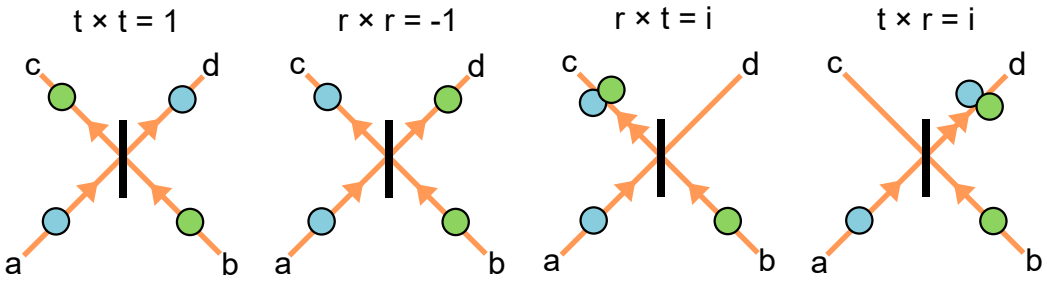

Figure 4.1: Two identical photons (same polarization, spatial distribution, spectrum) impinge onto a beam splitter at the same time. At the beam splitter interface, each photon can either reflect or transmit with probability amplitude r and t, respectively. There are four distinct possibilities, shown above. Treating each as a Feynman amplitude with a corresponding phase, two possibilities interfere destructively, leaving only the cases where the photons "bunch".

a nice physical interpretation in terms of an interference effect known as the Hong-Ou-Mandel effect. This is described below.

4.3 Hong-Ou-Mandel interference

Hong-Ou-Mandel (HOM) interference was an effect first observed in 1987 by researchers of the same name trying to measure subpicosecond timing intervals between photons [39]. However, it was later found to be a more general bosonic interference effect. Specifically, it is a fourth-order [2] interference effect that can occur with two indistinguishable bosons. It has been demonstrated using photons [39], surface plasmons [30], and bosonic atoms [51]. A typical photonic demonstration is achieved by sending two identical photons (same spatial distribution, polarization, spectrum) to arrive onto different ports of a beam splitter (BS) at the same time. This is described below using second quantization (assuming monochromatic photons for simplicity).

We consider two single photons in separate modes:

$$|\psi\rangle_{in} = \boldsymbol{a}^\dagger \boldsymbol{b}^\dagger |0\rangle_a |0\rangle_b = |1\rangle_a |1\rangle_b \tag{4.6}$$

[2] By fourth order, I mean that it is an interference effect involving four paths. As such, the interference involves quantities with the field amplitudes to the fourth order. In contrast, a Mach-Zender or Michelson interferometer involves only two paths and the field to second order.

These photons then impinge onto two ports of a BS, as in Fig. 4.1. The input-output relations of the BS are:

$$\begin{aligned} \boldsymbol{a} &\rightarrow (i\boldsymbol{c}+\boldsymbol{d})/\sqrt{2} \\ \boldsymbol{b} &\rightarrow (i\boldsymbol{d}+\boldsymbol{c})/\sqrt{2} \end{aligned} \tag{4.7}$$

where we chose the convention that a reflection gives rise to phase of $\pi/2$ (see Appendix C for details). Using these, we can find the state of the photons after they exit the BS:

$$\begin{aligned} |\psi\rangle_{out} &= \frac{1}{2}(i\boldsymbol{c}+\boldsymbol{d})^\dagger (i\boldsymbol{d}+\boldsymbol{c})^\dagger |0\rangle_c |0\rangle_d \\ &= \frac{1}{2}(-\boldsymbol{c}^\dagger \boldsymbol{d}^\dagger - i(\boldsymbol{d}^\dagger)^2 - i(\boldsymbol{c}^\dagger)^2 + \boldsymbol{c}^\dagger \boldsymbol{d}^\dagger)\,|0\rangle_c |0\rangle_d \\ &= \frac{-i}{2}((\boldsymbol{c}^\dagger)^2 + (\boldsymbol{d}^\dagger)^2)\,|0\rangle_c |0\rangle_d \\ &= \frac{-i}{\sqrt{2}}(|2\rangle_c |0\rangle_d + |0\rangle_c |2\rangle_d) \end{aligned} \tag{4.8}$$

This derivation is shown schematically in Fig. 4.1. When the two photons enter the BS, there are four possible outcomes that can occur. Since the output state is a superposition of all four, one should treat them like probability amplitudes (with their respective phases) and add them. In this way, it is easy to see that the cases where one photon transmits and the other reflects interfere destructively, leaving only the cases where the photons "bunch".

4.4 Optimal polarization cloner

But how can HOM interference be used for cloning? The strategy is shown schematically in Fig. 4.2. Here, we consider cloning a polarization state. The two input photons are identical in all other degrees of freedom.

One sends an unknown polarization state $|\psi\rangle$ (to be cloned) and an ancilla towards different ports of a BS. As mentioned earlier, the Buzek and Hillery cloner is made universal by choosing an ancilla that is in a completely mixed state:

$$\boldsymbol{a} = \frac{1}{2}(|\psi\rangle\langle\psi| + |\psi^\perp\rangle\langle\psi^\perp|) \tag{4.9}$$

This is sometimes referred to as "depolarized" light. More importantly, the ancilla is in a statistical mixture of being equal to the input state $|\psi\rangle$ half of the

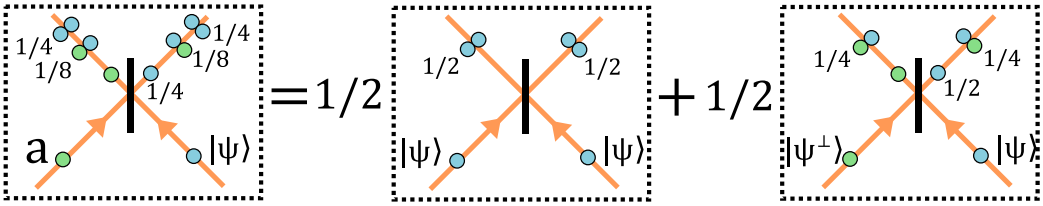

Figure 4.2: Schematic overview of Buzek and Hillery's optimal cloning with a beam splitter (BS). $|\psi\rangle$ is the state to be cloned, while $\boldsymbol{a} = \frac{1}{2}(|\psi\rangle\langle\psi| + |\psi^{\perp}\rangle\langle\psi^{\perp}|)$ is the ancilla. The cloning process is a statistical mixture of 50% of time having $|\psi\rangle$ as an input, and the other 50% of time having $|\psi^{\perp}\rangle$ as an input. The numbers within each box give the probability of that particular outcome to occur. By looking at cases where the photons bunch after the BS, we are twice as likely to have identical photons than orthogonal ones. This relative increase is due to HOM interference.

time, and being orthogonal to the input state the other half of the time, *i.e.* $\langle\psi^{\perp}|\psi\rangle = 0$.

The last ingredient of the Buzek and Hillery cloner is to perform a symmetric projection onto the two-photon input state. As it turns out [3], this corresponds to only considering cases where the photons exit the BS bunched. Let us examine this closer. Half the time, the ancilla is equal to $|\psi\rangle$ and so the two input photons are identical. In this case, owing to the HOM interference effect, the photons always bunch after the BS. The other half of the time, the ancilla is equal to $|\psi^{\perp}\rangle$, and so the two input photons are orthogonal to each other. In this case, there is no HOM interference, and so only a $1/2$ chance that the photons bunch. Thus, by looking only at bunching, we are twice as likely to get a contribution from the cases where the input photons were identical than when the photons were orthogonal. In this way, the symmetric projection improves the quality of the clones. It is surprising that this simple idea is the *best* possible cloning strategy in quantum mechanics!

Ultimately, we want to use this cloner to perform a joint measurement. That is, we want to simultaneously measure two non-commuting properties, one on each clone. The reader may foresee two possible issues. One is that the clones

[3] The only state that will never bunch at a BS is the anti-symmetric state, *i.e.* $|s\rangle = (|HV\rangle - |VH\rangle)/\sqrt{2}$ in the case of polarization. This state has fermionic behaviour, and consequently the photons do not want to be in the same mode. Hence, considering only the cases where the photons bunch is equivalent to projecting onto the symmetric part of the two-photon input state.

are not perfect copies of the input state, and so this may affect the joint measurement outcome. The second is that the measurements are still performed on separate clones, and so the strategy is insensitive to correlations between the measured properties. In the next chapter, I discuss an experiment where we overcome both of these issues. I will show that it is possible to mimic generating perfect copies with the Buzek and Hillery cloner. Furthermore, these perfect copies are entangled, thus providing the needed correlations between the measurement outcomes. These perfect and entangled copies are referred to as *twins*.

Chapter 5

Determining complementary properties with quantum twins

This chapter is based on the following publication:

G. S. Thekkadath, R. Y. Saaltink, L. Giner, J. S. Lundeen, "Determining complementary properties with quantum clones", *Phys. Rev. Lett*, **119** 050405 (2017)

5.1 Introduction

At the heart of quantum mechanics is the concept of complementarity: the impossibility of precisely determining complementary properties of a single quantum system. For example, a precise measurement of the position of an electron causes a subsequent momentum measurement to give a random result. Such joint measurements are the crux of Heisenberg's measurement-disturbance relation [67, 16], as highlighted by his famous microscope thought-experiment in 1927 [37]. Since then, methods for performing joint measurements of complementary properties have been steadily theoretically investigated [96, 5, 23, 12, 18], leading to seminal inventions such as heterodyne quantum state tomography [84, 50]. More recently, advances in the ability to control measurement-induced disturbance have led to ultra-precise measurements that surpass standard quantum limits [20], and also simultaneous determination of complementary properties with a precision that saturates Heisenberg's bound [78]. In sum, joint complementary measurements continue to prove useful for charac-

terizing quantum systems [55, 93, 6, 82] and for understanding foundational issues in quantum mechanics [78, 34, 20, 81].

We address the main challenge in performing a joint measurement, which is to circumvent the mutual disturbance caused by measuring two general non-commuting observables, $\boldsymbol{X}$ and $\boldsymbol{Y}$. Classically, such joint measurements (*e.g.* momentum and position) are sufficient to determine the state of the system, even of statistical ensembles. In quantum mechanics, these joint measurements have mainly been realized by carefully designing them to minimize their disturbance, such as in weak [55, 93, 6, 82, 81, 78] or non-demolition [12, 34, 20] measurements. In order to avoid these technically complicated measurements, one might instead consider manipulating the system, and in particular, copying it. Subsequently, one would perform a standard measurement separately on each copy of the system. Since the measurements are no longer sequential, or potentially not in the same location, one would not expect them to physically disturb one another. Crucially, as we explain below, the copies being measured must be correlated for this strategy to work. Hofmann recently proposed an experimental procedure that achieves this [38]. Following his proposal, we experimentally demonstrate that a partial-SWAP two-photon quantum logic gate [40] can isolate the measurement results of two photonic "twins". These twins are quantum-correlated (*i.e.* entangled) copies of a photon's polarization state that are ideal for performing joint measurements.

5.2 Theory

We begin by considering a physically impossible, but informative, strategy. Given a quantum system in a state $\boldsymbol{\rho}$, consider making two perfect copies $\boldsymbol{\rho} \otimes \boldsymbol{\rho}$ and then measuring observable $\boldsymbol{X}$ on copy one and $\boldsymbol{Y}$ on copy two. In this case, the joint probability of measuring outcomes $X = x$ and $Y = y$ is $\mathrm{Prob}(x, y) = \mathrm{Prob}(x)\mathrm{Prob}(y)$ [1]. Since it is factorable into functions of x and y, this joint probability cannot reveal correlations between the two properties. Even classically, this procedure would generally fail to give the system's state, since such correlations can occur in *e.g.* statistical ensembles. Less obviously, these correlations can occur in a single quantum system due to quantum coherence [96]. In turn, the lack of sensitivity to this coherence makes this joint measurement informa-

[1] As is usual for a probability, $\mathrm{Prob}(x, y)$ is estimated from repeated trials using an identical ensemble of input systems. This is implicit for probabilities and expectation values throughout the paper.

tionally incomplete [23], and thus this simplistic strategy is insufficient for determining quantum states [2]. Further confounding this strategy, the no-cloning theorem prohibits any operation that can create a perfect copy of an arbitrary quantum state, $\boldsymbol{\rho} \nrightarrow \boldsymbol{\rho} \otimes \boldsymbol{\rho}$ [98]. In summary, even if this strategy were allowed in quantum physics, it would not function well as a joint measurement.

Although perfect quantum copying is impossible, there has been extensive work investigating "cloners" that produce imperfect copies [83]. Throughout this paper, we consider a general "$1 \rightarrow 2$ cloner". It takes as an input an unknown qubit state $\boldsymbol{\rho}_a$ along with a blank ancilla $\boldsymbol{I}_b/2$ ($\boldsymbol{I}$ is the identity operator), and attempts to output two copies of $\boldsymbol{\rho}$ into separate modes, a and b.

We now consider a second strategy, one that utilizes a trivial version of this cloner by merely shuffling the modes of the two input states. This can be achieved by swapping their modes half of the time, and for the other half, leaving them unchanged. That is, one applies with equal likelihood the SWAP operation ($\boldsymbol{S}_{ab}$: $\boldsymbol{\rho}_a \boldsymbol{I}_b/2 \rightarrow \boldsymbol{I}_a \boldsymbol{\rho}_b/2$), or the identity operation ($\boldsymbol{I}_{ab} = \boldsymbol{I}_a \otimes \boldsymbol{I}_b$):

$$\boldsymbol{\rho}_a \boldsymbol{I}_b/2 \rightarrow (\boldsymbol{\rho}_a \boldsymbol{I}_b + \boldsymbol{I}_a \boldsymbol{\rho}_b)/4 \equiv \boldsymbol{t}_{ab}. \tag{5.1}$$

Each output mode of the trivial cloner $\boldsymbol{t}_{ab}$ contains an imperfect copy of the input state $\boldsymbol{\rho}$. Jointly measuring $\boldsymbol{X}$ and $\boldsymbol{Y}$, one on each trivial clone, yields the result $\text{Prob}(x, y) = (\text{Prob}(x) + \text{Prob}(y))/4$. In contrast to a joint measurement on perfect copies, this result exhibits correlations between x and y. These appear because in any given trial, only one of the observables is measured on $\boldsymbol{\rho}$, while the other is measured on the blank ancilla. Hence, the apparent correlations are an artifact caused by randomly switching the observable being measured, and are not due to genuine correlations that could be present in $\boldsymbol{\rho}$. While now physically allowed, this joint measurement strategy is still insufficient to determine the quantum state $\boldsymbol{\rho}$.

In order to access correlations in the quantum state, we must take advantage of quantum coherence. Instead of randomly applying $\boldsymbol{S}_{ab}$ or $\boldsymbol{I}_{ab}$ as in trivial cloning, we require the superposition of these two processes, *i.e.* the coherent sum:

$$\boldsymbol{\Pi}^j_{ab} = \frac{1}{2}(\boldsymbol{I}_{ab} + j\boldsymbol{S}_{ab}), \tag{5.2}$$

where now we are free to choose the phase j. $\boldsymbol{\Pi}^j$ is a generalized symmetry operation that can implement a partial-SWAP gate [40]. For $j = +1$ (-1), this

[2] The strategy considered here is informationally equivalent to separating an identical ensemble into two and measuring $\text{Prob}(x)$ with one half and $\text{Prob}(y)$ with the other half. Knowing only these two marginal distributions is insufficient to determine the quantum state [56].

operation is a projection onto the symmetric (anti-symmetric) part of the trivial cloner input, $\boldsymbol{\rho}_a \boldsymbol{I}_b/2$. The symmetric subspace only contains states that are unchanged by a SWAP operation. A projection onto this subspace increases the relative probability that $\boldsymbol{\rho}_a$ and the blank ancilla are identical. In fact, it has been proven that a symmetric projection on the trivial cloner input is the optimal cloning process, since it maximizes the fidelity of the clones (*i.e.* their similarity to $\boldsymbol{\rho}$) [15, 32, 14].

This brings us to our third and final strategy. Optimal cloning achieves more than just producing imperfect copies: the clones are quantum-correlated, *i.e.* entangled [15]. This can be seen by examining the output state of the optimal cloner (i.e. with $j = 1$):

$$\boldsymbol{o}^j_{ab} = \frac{2}{3}(\boldsymbol{\Pi}^j_{ab}\boldsymbol{\rho}_a \boldsymbol{I}_b \boldsymbol{\Pi}^{j\dagger}_{ab}) = \frac{2}{3}\boldsymbol{t}_{ab} + \frac{1}{3}\mathrm{Re}\left[j\boldsymbol{c}_{ab}\right], \tag{5.3}$$

where $\boldsymbol{c}_{ab} = \boldsymbol{S}_{ab}\boldsymbol{\rho}_a \boldsymbol{I}_b$ and $\mathrm{Re}[\mathbf{s}] = (\mathbf{s} + \mathbf{s}^\dagger)/2$. While the first term is two trivial clones, the second term is the coherent portion of the optimal clones, and is the source of their entanglement. Considered alone, $\boldsymbol{c}_{ab}$ corresponds to two "twins" of $\boldsymbol{\rho}$. Like perfect copies, any measurement on either twin gives results identical to what would be obtained with $\boldsymbol{\rho}$ [38]. However, the twins are entangled. As such, it is important to realize that they are very different from the uncorrelated perfect copies we considered in the first strategy. Relative to these (*i.e.* $\boldsymbol{\rho} \otimes \boldsymbol{\rho}$), performing the same joint measurement as before, but on the twins $\boldsymbol{c}_{ab}$, provides more information about $\boldsymbol{\rho}$. Measuring $\boldsymbol{X}$ on one twin and $\boldsymbol{Y}$ on the other yields the expectation value $\langle \boldsymbol{xy} \rangle_{\boldsymbol{\rho}} = \mathrm{Tr}(\boldsymbol{xy\rho})$, where $\boldsymbol{x} = |x\rangle\langle x|$ and $\boldsymbol{y} = |y\rangle\langle y|$ are projectors onto the eigenstates of observables $\boldsymbol{X}$ and $\boldsymbol{Y}$, respectively. Classically, this result would be interpreted as a joint probability $\mathrm{Prob}(x, y)$. However, due to Heisenberg's uncertainty principle, $\langle \boldsymbol{xy} \rangle_{\boldsymbol{\rho}}$ has non-classical features that shield precise determination of both $\boldsymbol{X}$ and $\boldsymbol{Y}$. In fact, $\langle \boldsymbol{xy} \rangle_{\boldsymbol{\rho}}$ is a "quasiprobability" distribution much like the Wigner distribution [96], and has similar properties such as being rigorously equivalent to the state $\boldsymbol{\rho}$ [6]. Unlike the Wigner distribution, it is generally complex since $\boldsymbol{xy}$ is not an observable (*i.e.* it is non-Hermitian). Although the measurements of $\boldsymbol{X}$ and $\boldsymbol{Y}$ are performed independently on each twin, because the twins are entangled, it is equivalent to simultaneously measuring the same two observables on a single copy of $\boldsymbol{\rho}$.

Performing a joint measurement directly on twins cannot be achieved in a physical process. This is likely part of the reason why previous theoretical investigations concluded that optimal cloners were not ideal for joint measure-

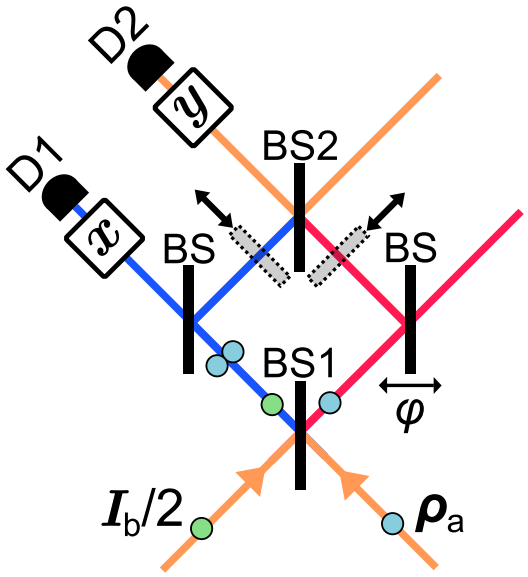

Figure 5.1: **Schematic of experimental setup.** A photon in a polarization state $\boldsymbol{\rho}_a$ and a photon in a blank state $\boldsymbol{I}_b/2$ enter an interferometer containing removable beam blocks (dotted outline). Complementary observables $\boldsymbol{x}$ and $\boldsymbol{y}$ are jointly measured by counting coincidences at detectors D1 and D2. When the red (blue) path is blocked, we post-select on the case where the photons exit the first beam splitter BS1 from the same (opposite) port and perform a symmetric projector $\boldsymbol{\Pi}^{+1}$ (anti-symmetric projector $\boldsymbol{\Pi}^{-1}$), thus making two optimal clones of $\boldsymbol{\rho}$. With no path blocked and a phase difference of $\varphi = \pm\pi/2$ between paths, we coherently combine both cases and perform $\boldsymbol{\Pi}^{\pm i}$, respectively.

ments [15, 21, 13]. However, in a joint measurement on optimal clones, Hofmann showed that the contribution from the twins can be isolated from that of the trivial clones [38]. This is because changing the phase j affects only the coherent part of the cloning process. Thus, by adding joint measurement results obtained from the optimal cloner with different phases j, we can isolate the contribution from the twins and measure $\langle \boldsymbol{x}\boldsymbol{y} \rangle_{\boldsymbol{\rho}}$ (see Sec. 5.4.2).

5.3 Results and discussion

The experiment is shown schematically in Fig. 5.1. A photonic system lends itself to optimal cloning because the symmetry operation $\boldsymbol{\Pi}^j$ in Eq. 5.2 can be

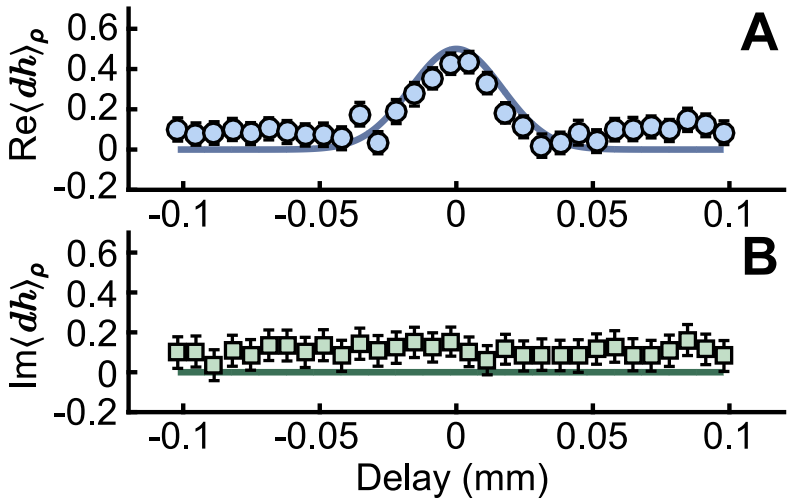

Figure 5.2: **Transition from trivial to optimal cloning.** A horizontal photon $\boldsymbol{\rho}_a = \boldsymbol{h}$ is sent into the cloner. We jointly measure complementary observables $\boldsymbol{d}$ and $\boldsymbol{h}$, one on each clone, and plot the real (**A**) and imaginary (**B**) parts of $\langle \boldsymbol{dh} \rangle_{\boldsymbol{\rho}}$. For large delays, only trivial clones are produced. Since they contain no information about $\langle \boldsymbol{dh} \rangle_{\boldsymbol{\rho}}$, our procedure cancels their contribution to the joint measurement result. At zero delay, optimal clones are produced. We isolate the contribution of the twins to the joint measurement, yielding the desired value of $\langle \boldsymbol{dh} \rangle_{\boldsymbol{\rho}} = 0.5$. The bold lines are theory curves calculated for intermediate delays (see Sec. 5.4.2). Error bars are calculated using Poissonian counting statistics.

implemented with a beam splitter (BS). If two indistinguishable photons impinge onto different ports of BS1, Hong-Ou-Mandel interference occurs and the photons always "bunch" by exiting BS1 from a single port. By selecting cases where photons bunch (anti-bunch), one implements the symmetry projector $\boldsymbol{\Pi}^{+1}$ ($\boldsymbol{\Pi}^{-1}$) [17]. This enabled previous experimental demonstrations of optimal cloners for both polarization [42] and orbital angular momentum [63, 11] states. However, we must also implement $\boldsymbol{\Pi}^{\pm i}$. Following a similar strategy as Refs. [40, 57], we use an interferometer to coherently combine the symmetric and anti-symmetric projectors, since $\boldsymbol{\Pi}^{\pm i} = (e^{\pm i\pi/4}\boldsymbol{\Pi}^{+1} + e^{\mp i\pi/4}\boldsymbol{\Pi}^{-1})/\sqrt{2}$. This is achieved by interfering at BS2 the cases where the photons bunched at BS1 with cases where they anti-bunched at BS1. In summary, this provides an experimental procedure to vary the phase j and thereby isolate the joint measurement contribution of the twins from that of the trivial clones.

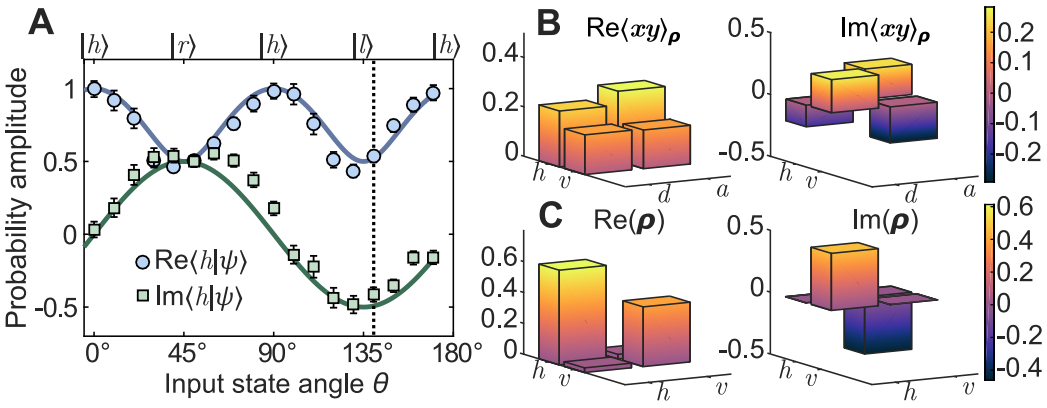

Figure 5.3: **Measuring the quantum state.** Various polarization states $|\psi\rangle = \alpha|h\rangle + \beta|v\rangle$ are produced by rotating the fast-axis angle θ of a quarter-wave plate with increments of 10°. We plot the real and imaginary parts of $\alpha = \langle h|\psi\rangle = \sqrt{\frac{3}{8}\cos(4\theta) + \frac{5}{8}} + i\sin\theta\cos\theta$ in **A** (theory is bold lines, $|r\rangle = (|v\rangle + i|h\rangle)/\sqrt{2}$ and $|l\rangle = (|v\rangle - i|h\rangle)/\sqrt{2}$ are circular polarizations). Error bars are calculated using Poissonian counting statistics. The entire joint quasiprobability distribution (**B**) and density matrix (**C**) are also shown for the input state indicated by the dashed line (color represents amplitude). After processing the counts with a maximum-likelihood estimation, the average fidelity $\left|\langle\psi|\boldsymbol{\rho}|\psi\rangle\right|^2$ of the 18 measured states is 0.92 ± 0.05.

We experimentally verify that this procedure works by performing a joint measurement on trivial clones $\boldsymbol{t}_{ab}$ and showing that its outcome does not contribute to $\langle \boldsymbol{xy}\rangle_{\boldsymbol{\rho}}$. In particular, we scan the delay between $\boldsymbol{\rho}_a$ and $\boldsymbol{I}_b/2$ at BS1. When the delay is zero, we implement the symmetry operator $\boldsymbol{\Pi}^j$. When the delay is larger than the coherence time of the photons, the BS does not discriminate the symmetry of the two-qubit input state. Thus, it simply shuffles the modes of both qubits and produces trivial clones $\boldsymbol{t}_{ab}$. We test the procedure by measuring $\langle \boldsymbol{xy}\rangle_{\boldsymbol{\rho}} = \langle \boldsymbol{dh}\rangle_{\boldsymbol{\rho}}$, where $\boldsymbol{d}$ and $\boldsymbol{h}$ are diagonal and horizontal polarization projectors, respectively. We use an input state $\boldsymbol{\rho}_a = \boldsymbol{h}$, for which one expects $\langle \boldsymbol{dh}\rangle_{\boldsymbol{\rho}} = \mathrm{Tr}(\boldsymbol{dhh}) = 0.5$. In Fig. 5.2, we show that for large delays $\langle \boldsymbol{dh}\rangle_{\boldsymbol{\rho}} = 0$, whereas for zero delay, it obtains its full value. This shows that the procedure has effectively removed the contribution of the trivial clones to the optimal clone state in Eq. 5.3, and so the joint measurement result is solely due to the twins.

A joint measurement on twins of $\boldsymbol{\rho}$ can reveal correlations between complementary properties in $\boldsymbol{\rho}$. We measure the entire joint quasiprobability distribution $\langle \boldsymbol{x}\boldsymbol{y} \rangle_{\boldsymbol{\rho}}$ for the complementary polarization observables $\boldsymbol{x} = \{\boldsymbol{d}, \boldsymbol{a}\}$ using diagonal and anti-diagonal projectors, and $\boldsymbol{y} = \{\boldsymbol{h}, \boldsymbol{v}\}$ using horizontal and vertical projectors. This is repeated for a variety of different input states $\boldsymbol{\rho}$. For the input state indicated by the dashed line in Fig. 5.3A, correlations can be seen in $\mathrm{Im}\langle \boldsymbol{x}\boldsymbol{y} \rangle_{\boldsymbol{\rho}}$, as shown in Fig. 5.3B. With the ability to exhibit correlations, $\langle \boldsymbol{x}\boldsymbol{y} \rangle_{\boldsymbol{\rho}}$ is now a complete description of the quantum state $\boldsymbol{\rho}$ (see Sec. 5.4.2). In particular, the wave function of the state (see Fig. 5.3A) is any cross-section of $\langle \boldsymbol{x}\boldsymbol{y} \rangle_{\boldsymbol{\rho}}$. Moreover, the density matrix (see Fig. 5.3C) can be obtained with a Fourier transform of $\langle \boldsymbol{x}\boldsymbol{y} \rangle_{\boldsymbol{\rho}}$. This is the key experimental result. In the classical world, simultaneously measuring complementary properties gives the system's state. This result demonstrates that simultaneously measuring complementary observables on twins, similarly, gives the system's state.

In addition to its fundamental importance, our result has potential practical advantages as a state determination procedure. It is valid for higher dimensional states (see Sec. 5.4.2) for which standard quantum tomography requires prohibitively many measurements. In contrast, here the wave function and density matrix are obtained directly (*i.e.* without a reconstruction algorithm) from experimental measurements of only two observables, $\boldsymbol{X}$ and $\boldsymbol{Y}$.

Our results uncover striking connections with other joint measurements techniques, despite the physics of each approach being substantially different. For example, the joint quasiprobability $\langle \boldsymbol{x}\boldsymbol{y} \rangle_{\boldsymbol{\rho}}$ is also the average outcome of another joint measurement strategy: the weak measurement of $\boldsymbol{y}$ followed by a measurement of $\boldsymbol{x}$ on a single system $\boldsymbol{\rho}$ [82, 6, 38]. Furthermore, in the continuous-variable analogue of our work, measurements of complementary observables on cloned Gaussian states [83] give a different, but related, quasiprobability distribution for the quantum state known as the Q-function [50]. These connections emphasize the central role of optimal cloning in quantum mechanics [98, 14] and clarify the intimate relation between joint measurements of complementary observables and determining quantum states [96, 23].

We anticipate that simultaneous measurements of non-commuting observables can be naturally implemented in quantum computers using our technique, since the operation $\boldsymbol{\Pi}^j$ can be achieved using a controlled-SWAP quantum logic gate [38, 70]. As joint measurements are pivotal in quantum mechanics, this will have broad implications for state estimation [55, 93, 6, 82], quantum control [34], and quantum foundations [81, 78]. For instance, we anticipate that our method can be used to efficiently and directly measure high-

dimensional quantum states that are needed for fault-tolerant quantum computing and quantum cryptography [11].

5.4 Methods

5.4.1 Experimental setup

A detailed figure containing the experimental setup is shown in Fig. 5.4. A 40 mW continuous-wave diode laser at 404 nm pumps a type-II β-barium borate crystal. Through spontaneous parametric down-conversion, pairs of 808 nm photons with orthogonal polarization are generated collinearly with the pump laser. The latter is then blocked by a long pass filter. The photon pair splits at a polarizing beam splitter (PBS), and each photon is coupled into a polarization-maintaining single mode fiber. The path length difference between the photon paths is adjusted with a delay stage. A spinning (2 Hz) half-wave plate produces a completely mixed state $\boldsymbol{I}/2$ at one fiber output, while a half-wave plate and quarter-wave plate produce the state $\boldsymbol{\rho}$ to be cloned at the other fiber output. A displaced Sagnac interferometer composed of two BS is used instead of the interferometer in Fig. 5.1h, since it is more robust to air fluctuations and other instabilities. The phase φ between red and blue paths is adjusted by slightly rotating one of the mirrors in the interferometer in order to change the path length difference between both paths. A series of wave plates and a PBS are used to implement the projectors $\boldsymbol{x}$ and $\boldsymbol{y}$. Detectors are single photon counting silicon avalanche photodiodes. Using time-correlation electronics, we count coincidence events that occur in a 5 nanosecond window and average over 60 seconds for each measurement.

5.4.2 Joint measurement on optimal clones

For qudits, the d-dimensional observables $\boldsymbol{X}$ and $\boldsymbol{Y}$ are complementary if their eigenstates $\{|x\rangle\}$ and $\{|y\rangle\}$ all satisfy $\left|\langle x|y\rangle\right| = 1/\sqrt{d}$. We use the notation $\boldsymbol{x} = |x\rangle\langle x|$. The output of an optimal cloner for qudits is:

$$\boldsymbol{o}_{ab}^{j} = \frac{2}{d+1}\left(\boldsymbol{\Pi}_{ab}^{j}\boldsymbol{\rho}_{a}\boldsymbol{I}_{b}\boldsymbol{\Pi}_{ab}^{j\dagger}\right) \tag{5.4}$$

with $j = +1$. Consider measuring $\boldsymbol{X}$ in mode a and $\boldsymbol{Y}$ in mode b. As shown in Ref. [38], the joint probability of measuring outcome $X = x$ and $Y = y$ is:

$$\begin{aligned} \text{Prob}^j(x,y) &= \text{Tr}\left[\boldsymbol{x}_a \boldsymbol{y}_b \boldsymbol{o}^j_{ab}\right] \\ &= \frac{1}{2(d+1)}\left(\langle \boldsymbol{x}\rangle_{\boldsymbol{\rho}} + \langle \boldsymbol{y}\rangle_{\boldsymbol{\rho}} + 2\text{Re}\left(j\,\langle \boldsymbol{x}\boldsymbol{y}\rangle_{\boldsymbol{\rho}}\right)\right). \end{aligned} \tag{5.5}$$

The terms $\langle \boldsymbol{x}\rangle_{\boldsymbol{\rho}}$ and $\langle \boldsymbol{y}\rangle_{\boldsymbol{\rho}}$ could be obtained from a joint measurement on trivial clones. In contrast, the last term $\langle \boldsymbol{x}\boldsymbol{y}\rangle_{\boldsymbol{\rho}}$ is obtained from a joint measurement on twins, and is a joint quasiprobability of simultaneously measuring both $\boldsymbol{x}$ and $\boldsymbol{y}$ on $\boldsymbol{\rho}$. In order to isolate the latter term, we use the fact that the joint measurement contribution of the trivial clones does not depend on the phase j, giving:

$$\langle \boldsymbol{x}\boldsymbol{y}\rangle_{\boldsymbol{\rho}} = \frac{d+1}{2} \sum_{j=\pm 1,\pm i} j^* \text{Prob}^j(x,y). \tag{5.6}$$

When the input state is pure, that is $\boldsymbol{\rho} = |\psi\rangle\langle\psi|$, then $\langle \boldsymbol{x}\boldsymbol{y}\rangle_{\psi} = \nu\,\langle y|\psi\rangle$, where $\nu = \langle\psi|x\rangle\langle x|y\rangle$. For some $x = x_0$, the phase of ν is constant for all y and so the wave function $|\psi\rangle$ can be expressed in the basis of $\boldsymbol{Y}$ as $|\psi\rangle = \frac{1}{\nu}\sum_y \langle \boldsymbol{x_0}\boldsymbol{y}\rangle_{\psi}|y\rangle$. As usual, the constant ν is found by normalizing $|\psi\rangle$. Thus, using Eq. 5.6, any complex amplitude $\psi(y) = \langle y|\psi\rangle$ of the wave function can be found from:

$$\psi(y) = \frac{d+1}{2\nu} \sum_{j=\pm 1,\pm i} j^* \text{Prob}^j(x_0,y). \tag{5.7}$$

The choice of x_0 is equivalent to choosing a phase reference for the wave function. In Fig. 5.3A, we use $x_0 = d$, which defines the diagonal polarization as $|d\rangle = (|h\rangle + |v\rangle)/\sqrt{2}$. We choose to make the normalization constant ν a real number, *i.e.* $\nu = (|\langle \boldsymbol{d}\boldsymbol{h}\rangle|^2 + |\langle \boldsymbol{d}\boldsymbol{v}\rangle|^2)^{1/2}$.

For mixed input states, the joint quasiprobability $\langle \boldsymbol{x}\boldsymbol{y}\rangle_{\boldsymbol{\rho}}$ is related to the density matrix $\boldsymbol{\rho}$ via a discrete Fourier transform (see derivation below).

5.4.3 Relating the joint quasiprobability to the density matrix

Here we summarize the connection between the joint quasiprobability distribution and the density matrix. Consider the d-dimensional complementary observables $\boldsymbol{X}$ and $\boldsymbol{Y}$ with eigenstates $\{x_i\}$ and $\{y_i\}$ such that $\left|\langle x_i|y_j\rangle\right| = 1/\sqrt{d}$ for any i, j. Without loss of generality [29], one can take the $\{y_i\}$ basis to be

defined in terms of a discrete Fourier transform of $\{x_i\}$:

$$|y_j\rangle = \sum_{i=0}^{d-1} |x_i\rangle \exp(i2\pi x_i y_j/d)/\sqrt{d}. \tag{5.8}$$

This fixes a phase relation for the inner product of all the eigenstates of both bases:

$$\langle x_i|y_j\rangle = \exp(i2\pi x_i y_j)/\sqrt{d}. \tag{5.9}$$

A general d-dimensional quantum state $\boldsymbol{\rho}$ can be written in the basis of $\boldsymbol{Y}$ as $\boldsymbol{\rho} = \sum_{k,l} p_{kl} |y_k\rangle \langle y_l|$. We wish to relate the coefficients p_{kl} to the joint quasiprobability distribution, *i.e.* $\langle \boldsymbol{xy} \rangle_{\boldsymbol{\rho}}$. Recall that we use the notation $\boldsymbol{x} = |x\rangle \langle x|$. Thus $\langle \boldsymbol{xy} \rangle_{\boldsymbol{\rho}}$ takes the form of $D_{ij} \equiv \langle |x_i\rangle \langle x_i|y_j\rangle \langle y_j| \rangle_{\boldsymbol{\rho}} = \mathrm{Tr}\left[|x_i\rangle \langle x_i|y_j\rangle \langle y_j| \boldsymbol{\rho}\right] = \langle x_i|y_j\rangle \langle y_j|\boldsymbol{\rho}|x_i\rangle$. Inserting the expanded form of $\boldsymbol{\rho}$:

$$\begin{aligned} D_{ij} = \langle x_i|y_j\rangle \langle y_j| \sum_{k,l} p_{kl} |y_k\rangle \langle y_l|x_i\rangle &= \langle x_i|y_j\rangle \sum_l p_{jl} \langle y_l|x_i\rangle \\ &= \frac{\exp(i2\pi x_i y_j)}{d} \sum_{l=0}^{d-1} p_{jl} \exp(-i2\pi x_i y_l). \end{aligned} \tag{5.10}$$

This shows that the joint quasiprobability is the discrete Fourier transform of the density matrix. The equation can be inverted by taking the inverse Fourier transform of both sides:

$$p_{jl} = \sum_{i=0}^{d-1} D_{ij} \exp(i2\pi x_i (y_l - y_j)). \tag{5.11}$$

In the case of polarization qubits, $\boldsymbol{x} = \{\boldsymbol{d}, \boldsymbol{a}\}$ and $\boldsymbol{y} = \{\boldsymbol{h}, \boldsymbol{v}\}$. Then the equation relating the two density matrix and the joint quasiprobability is:

$$\boldsymbol{\rho} = \begin{pmatrix} \langle \boldsymbol{dh} \rangle_{\boldsymbol{\rho}} + \langle \boldsymbol{ah} \rangle_{\boldsymbol{\rho}} & \langle \boldsymbol{dh} \rangle_{\boldsymbol{\rho}} - \langle \boldsymbol{ah} \rangle_{\boldsymbol{\rho}} \\ \langle \boldsymbol{dv} \rangle_{\boldsymbol{\rho}} - \langle \boldsymbol{av} \rangle_{\boldsymbol{\rho}} & \langle \boldsymbol{dv} \rangle_{\boldsymbol{\rho}} + \langle \boldsymbol{av} \rangle_{\boldsymbol{\rho}} \end{pmatrix}. \tag{5.12}$$

Eq. 5.12 is used to calculate the density matrix in Fig. 5.3C.

5.4.4 Trivial to optimal clones

When the two input photons are temporally distinguishable, Hong-Ou-Mandel interference does not occur at the first beam splitter, and the cloner produces trivial clones $\boldsymbol{t}_{ab}$. Conversely, for temporally indistinguishable photons, we

produce $\boldsymbol{o}^{j}_{ab}$. Photons that are partially distinguishable can be decomposed into the form

$$\boldsymbol{\sigma}^{j}_{ab} = |\alpha|^2 \boldsymbol{o}^{j}_{ab} + (1-|\alpha|^2)\boldsymbol{t}_{ab}, \tag{5.13}$$

where $\alpha \in [0,1]$ is a temporal distinguishability factor. In particular, the temporal mode of the delayed photon in mode a can be written as:

$$|\zeta_a\rangle = \int d\omega \phi(\omega) e^{-i\omega\tau} a^{\dagger}(\omega)|0\rangle, \tag{5.14}$$

where τ is the delay, while the other photon in mode b is described by $|\zeta_b\rangle = \int d\omega \phi(\omega) b^{\dagger}(\omega)|0\rangle$. For a Gaussian spectral amplitude $\phi(\omega) = \frac{1}{\sqrt{\pi}\Delta\omega} e^{\frac{-(\omega-\omega_0)^2}{2\Delta\omega^2}}$ where ω_0 is the central frequency of the photons and $\Delta\omega$ is their spectral width, the distinguishability factor is given by

$$|\alpha|^2 = |\langle\zeta_a|\zeta_b\rangle|^2 = e^{\frac{-\Delta\omega^2\tau^2}{2}}. \tag{5.15}$$

In the experiment, we adjust the delay τ by moving the delay stage. The parameter $\Delta\omega^2$ is extracted from fitting a Gaussian to the Hong-Ou-Mandel dip (see Fig. 5.5).

5.4.5 Additional figures

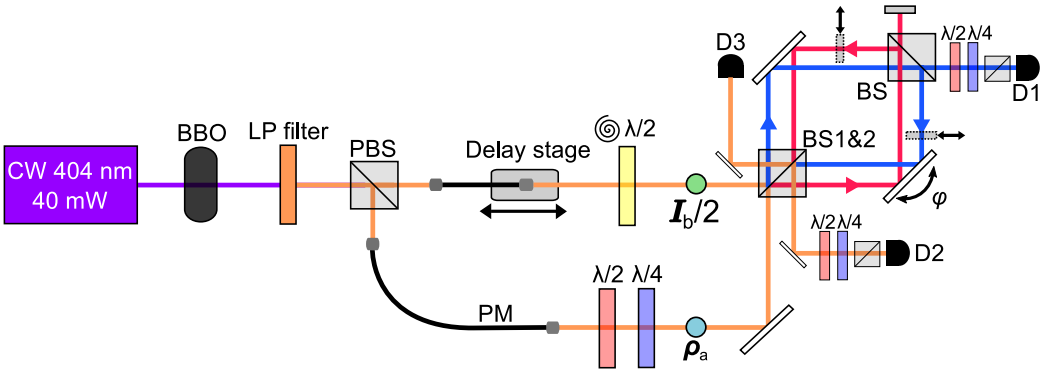

Figure 5.4: **Experimental setup.** Details of the experimental setup can be found in the Methods section. A simplified schematic of this setup is shown in Fig. 5.1. Detector D3 is used for alignment purposes, but otherwise is not used in the experiment. CW: continuous-wave, BBO: β-barium borate, LP: long pass, (P)BS: (polarizing) beam splitter, PM: polarization-maintaining, $\lambda/2$: half-wave plate, $\lambda/4$: quarter-wave plate, D: avalanche photodiode detector.

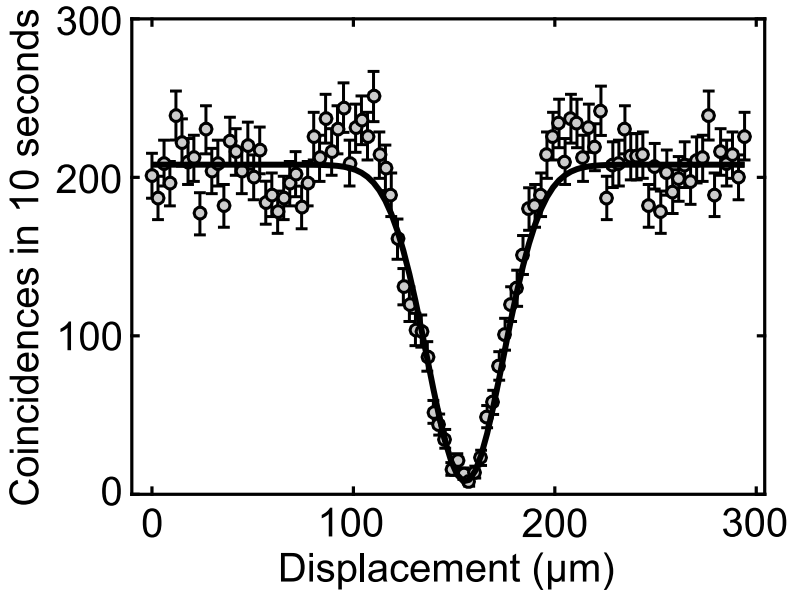

Figure 5.5: **Hong-Ou-Mandel interference.** In order to characterize the spectral width of the photons and to ensure that we are performing the symmetry projector $\mathbf{\Pi}_{ab}^{\pm 1}$, we measure the width and visibility of the Hong-Ou-Mandel dip at BS1. With both input photons horizontally polarized and the blue path blocked, we measure the number of coincidences at detectors D1 and D2 as a function of the position of the delay stage. The visibility $\mathcal{V} = (C_{max} - C_{min})/(C_{max} + C_{min})$ (where C is the number of coincidences) of the dip is $\sim 96\%$. Error bars are calculated using Poissonian counting statistics.

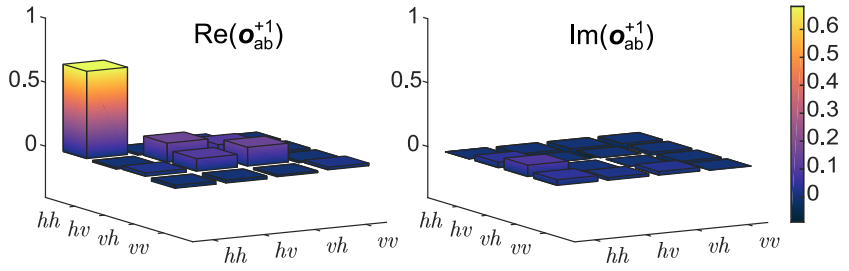

Figure 5.6: **Quantum state tomography of $\mathbf{\Pi}^{+1}_{ab}$ output.** In order to determine the fidelity of our clones, we perform two-photon quantum state tomography on the output $\boldsymbol{o}^{+1}_{ab}$ of the cloner. Here the input state to be cloned is $\boldsymbol{\rho}_a = \boldsymbol{h}$. By tracing over each subsystem of the measured $\boldsymbol{o}^{+1}_{ab}$, we can compute the fidelities $F_a = \left|\langle h|\boldsymbol{o}^{+1}_a|h\rangle\right|^2$ and $F_b = \left|\langle h|\boldsymbol{o}^{+1}_b|h\rangle\right|^2$. We obtain $F_a = 0.832$ and $F_b = 0.829$, which nearly saturates the theoretical bound of $5/6 \sim 0.833$.

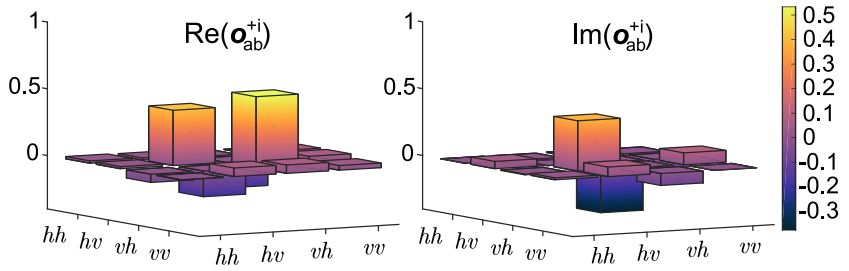

Figure 5.7: **Quantum state tomography of $\mathbf{\Pi}^{+i}_{ab}$ output.** In order to achieve the $\mathbf{\Pi}^{+i}_{ab}$ operation, both paths in the interferometer are unblocked and the phase between them is $\varphi = \pi/2$. We test our ability to implement $\mathbf{\Pi}^{+i}_{ab}$ by performing two-photon quantum state tomography on the state after the $\mathbf{\Pi}^{+i}_{ab}$ operation. As an input, we use the state $|hv\rangle\langle hv|$. In this case, the fidelity of the output state $\boldsymbol{o}^{+i}_{ab}$ is 0.850.

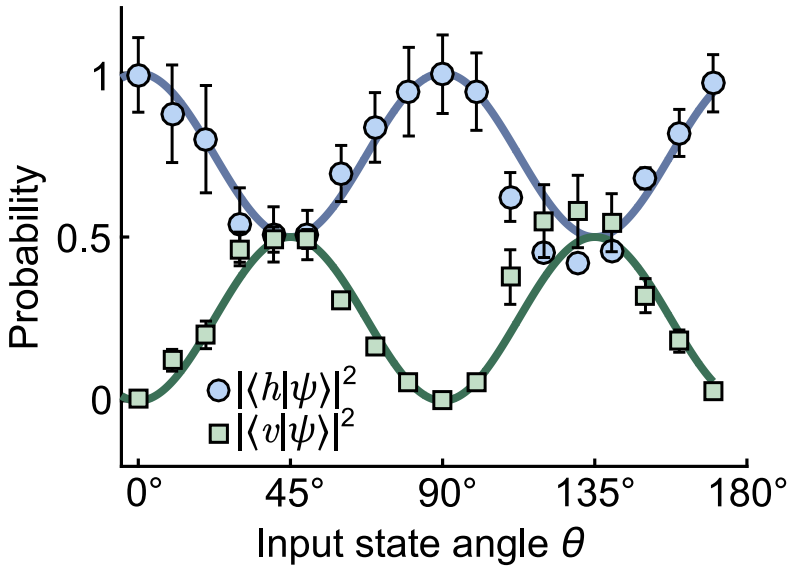

Figure 5.8: **Absolute value squared of the measured wave function.** The data in this figure is the same as the data used in Fig. 5.3. The polarization state of the input photon as a function of the the quarter wave-plate fast-axis can be written in the form $|\psi\rangle = \alpha|h\rangle + \beta|v\rangle$. Here we plot both $|\alpha|^2 = \cos^4\theta + \sin^4\theta$ and $|\beta|^2 = 2\sin^2\theta\cos^2\theta$ (theory is bold lines). Error bars are calculated using Poissonian counting statistics.

Chapter 6

Conclusions

6.1 Summary

This thesis investigated joint measurements, which lie at the intersection of the Heisenberg uncertainty principle and measurement disturbance in quantum mechanics. Both of these concepts involve non-commuting properties, and both refer to a limit in the precision with which these properties can be determined. However, measurement disturbance is circumventable, whereas the uncertainty principle is not. We described and experimentally implemented two strategies that achieved this, namely weak measurements and quantum cloning. In the former, the strength of the measurement is reduced as to also reduce its disturbance. In the latter, the system is first copied so that each measurement is performed on a separate copy. I would argue that these are both "naive" strategies in the sense that they are based on simple ideas. Surprisingly, they both function well as joint measurements. Notably, both strategies allow us to recover some intuition from the world of classical physics, and directly measure states by simultaneously measuring their complementary properties.

However, the devil, or the "quantumness", is in the detail of these measurement strategies. In the weak measurement case, one entangles the system being measured with a pointer through an interaction which depends on the measured property. Although only the pointer is measured, this entanglement mediates measurement disturbance on the system, and hence must be minimized. We implemented a joint measurement by performing a sequence of such weak measurements, each requiring their own pointer. Correlations between the pointers revealed correlations between the measured properties. In

the cloning case, we used quantum coherence to isolate “twins" from the output of an optimal cloner (which itself relied on a quantum interference effect known as Hong-Ou-Mandel interference). These twins are perfect and entangled copies of the cloner input system. We implemented a joint measurement by simultaneously measuring complementary properties, one on each twin. The entanglement between the twins was paramount to reveal correlations between the complementary properties.

Although joint measurements have a long history, their central role in quantum mechanics has been largely overlooked. Despite there being theoretical proposals as early as 1965 [5], experiments were lacking. Luckily, there has been a renewed interest in the topic thanks to recent experimental developments. Now, both non-demolition and weak measurements are commonly used to implement joint measurements in optics [55], atomic [20], and superconducting [34] physics labs. With these, physicists are refining their understanding of foundational concepts such as the Heisenberg uncertainty principle [81], performing measurements of exquisite precision [20], and characterizing quantum states more directly and efficiently than before [55]. Surely, there are many other potential applications for joint measurements. Perhaps with the current renewed interest, these will be explored further. Before concluding, I discuss a few which I find particularly interesting.

6.2 Future work

The number of schemes to implement joint measurements is steadily growing. It now includes weak and non-demolition measurements, eight-port homodyne, and quantum cloning. There is a connection between all of these which has yet to be made clear. For example, a simultaneous measurement on twins gives exactly the same result as two sequential weak measurements, namely the weak average. Furthermore, eight-port homodyne can be viewed as an optimal cloner, except the ancilla is replaced by vacuum noise entering the unused port of the beam splitter. This is completely analogous to the strategy used in Ch. 5. The physics behind of each of these strategies is quite different. Thus, if the connections (and the reason that they are there) can be understood more clearly, this may be useful for developing additional joint measurement strategies. Perhaps these connections will be revealed if all the strategies are analyzed within a single framework, namely using a generalized measurement formalism such as POVMs.

The prospect of performing joint measurements beyond two observables is an interesting one. One strategy to experimentally implement such a joint measurement is to extend the idea used in Ch. 3 and perform a large sequence of weak measurements. Some researchers are trying this approach [74]. A major issue is that a separate pointer is needed for each observable, and correlations between all of these pointers need to be measured (2^N measurements for a joint measurement of N observables). Extending the cloning strategy may also be possible. There has not yet been an experimental demonstration of an optimal $1 \rightarrow N$ cloner for $N > 2$, despite there being a theoretical proposal as early as in 2000 by C. Simon *et al.* [88]. In any case, one would still then need to figure out how to isolate not twins, but "$N-$tuplets", from this cloner. Presumably, this process would also require 2^N measurements.

One reason that this is an interesting prospect was briefly discussed in Sec. 2.3.3: large joint measurements can be used to better understand the role of time, and its connection to measurement (*e.g.* operator ordering), in quantum mechanics. Besides being of philosophical interest, this could provide insight into the *problem of time*, which refers to a major conceptual conflict when reconciling quantum mechanics with general relativity. Operator ordering plays an important role in joint measurements. In Ch. 2, we saw that the ordering of non-commuting operators affects the result of a weak measurement sequence. For instance, reversing the order gives the complex conjugate of the weak average. In contrast, in the cloning experiment of Ch. 5, there is no "ordering" in the joint measurement, since the measurements are performed simultaneously in time. In that case, the imaginary part of the joint measurement result vanishes, and must be recovered using an interferometer. Moreover, a recent paper using non-demolition measurements also emphasizes the importance of "keeping track of the time ordering record" in their joint measurements [34]. Indeed, some theorists have already started to formalize the role of operator ordering and time in the context of weak measurements [8]. But, it has not yet been accomplished within the larger context of joint measurements.

Bibliography

[1] Left image taken from A.C. Miracle and S.K. Mukherji, *AJNR Am. J. Neuroradiol.* **30** 1088-1096 (2009). ©2009 American Society of Neuroradiology. Right image taken from Institute for Quantum Science Technology http://www.iqst.ca/quantech/research/fock.php.

[2] Christoph Adami and Greg Ver Steeg. Black holes are almost optimal quantum cloners. *J. Phys. A*, 48(23):23FT01, 2015.

[3] Yakir Aharonov, David Z. Albert, and Lev Vaidman. How the result of a measurement of a component of the spin of a spin-1/2 particle can turn out to be 100. *Phys. Rev. Lett.*, 60:1351–1354, Apr 1988.

[4] Yakir Aharonov and Lev Vaidman. Properties of a quantum system during the time interval between two measurements. *Phys. Rev. A*, 41:11–20, Jan 1990.

[5] E. Arthurs and J. L. Kelly. On the simultaneous measurement of a pair of conjugate observables. *Bell Syst. Tech. J.*, 44(4):725–729, 1965.

[6] Charles Bamber and Jeff S. Lundeen. Observing dirac's classical phase space analog to the quantum state. *Phys. Rev. Lett.*, 112:070405, Feb 2014.

[7] A. O. Barut. Distribution functions for noncommuting operators. *Phys. Rev.*, 108:565–569, Nov 1957.

[8] Adam Bednorz, Kurt Franke, and Wolfgang Belzig. Noninvasiveness and time symmetry of weak measurements. *New Journal of Physics*, 15(2):023043, 2013.

[9] N. Bent, H. Qassim, A. A. Tahir, D. Sych, G. Leuchs, L. L. Sánchez-Soto, E. Karimi, and R. W. Boyd. Experimental realization of quantum tomography of photonic qudits via symmetric informationally complete positive operator-valued measures. *Phys. Rev. X*, 5:041006, Oct 2015.

[10] Eliot Bolduc, Genevieve Gariepy, and Jonathan Leach. Direct measurement of large-scale quantum states via expectation values of non-hermitian matrices. *Nat. Commun.*, 7, 2016.

[11] Frédéric Bouchard, Robert Fickler, Robert W. Boyd, and Ebrahim Karimi. High-dimensional quantum cloning and applications to quantum hacking. *Science Adv.*, 3(2), 2017.

[12] Vladimir B. Braginsky, Yuri I. Vorontsov, and Kip S. Thorne. Quantum nondemolition measurements. *Science*, 209(4456):547–557, 1980.

[13] Thomas Brougham, Erika Andersson, and Stephen M. Barnett. Cloning and joint measurements of incompatible components of spin. *Phys. Rev. A*, 73:062319, Jun 2006.

[14] Dagmar Bruss, Artur Ekert, and Chiara Macchiavello. Optimal universal quantum cloning and state estimation. *Phys. Rev. Lett.*, 81:2598–2601, Sep 1998.

[15] V. Bužek and M. Hillery. Quantum copying: Beyond the no-cloning theorem. *Phys. Rev. A*, 54:1844–1852, Sep 1996.

[16] Paul Busch, Pekka Lahti, and Reinhard F. Werner. Colloquium: Quantum root-mean-square error and measurement uncertainty relations. *Rev. Mod. Phys.*, 86:1261–1281, Dec 2014.

[17] Richard A. Campos and Christopher C. Gerry. Permutation-parity exchange at a beam splitter: Application to heisenberg-limited interferometry. *Phys. Rev. A*, 72:065803, Dec 2005.

[18] Claudio Carmeli, Teiko Heinosaari, and Alessandro Toigo. Informationally complete joint measurements on finite quantum systems. *Phys. Rev. A*, 85:012109, Jan 2012.

[19] Leon Cohen. *Time-frequency Analysis: Theory and Applications*. Prentice-Hall, Inc., Upper Saddle River, NJ, USA, 1995.

[20] Giorgio Colangelo, Ferran Martin Ciurana, Lorena C. Bianchet, Robert J. Sewell, and Morgan W. Mitchell. Simultaneous tracking of spin angle and amplitude beyond classical limits. *Nature*, 543(7646):525–528, Mar 2017.

[21] G M D'Ariano, C Macchiavello, and M F Sacchi. Joint measurements via quantum cloning. *J. Opt. B: Quantum Semiclass. Opt.*, 3(2):44, 2001.

[22] G. M. D'Ariano and H. P. Yuen. Impossibility of measuring the wave function of a single quantum system. *Phys. Rev. Lett.*, 76:2832–2835, Apr 1996.

[23] Willem M. de Muynck, Peter A. E. M. Janssen, and Alexander Santman. Simultaneous measurement and joint probability distributions in quantum mechanics. *Found. Phys.*, 9(1):71–122, 1979.

[24] Antonio Di Lorenzo. Sequential measurement of conjugate variables as an alternative quantum state tomography. *Phys. Rev. Lett.*, 110(1):010404, 2013.

[25] P. A. M. Dirac. On the analogy between classical and quantum mechanics. *Rev. Mod. Phys.*, 17:195–199, Apr 1945.

[26] P. Ben Dixon, David J. Starling, Andrew N. Jordan, and John C. Howell. Ultrasensitive beam deflection measurement via interferometric weak value amplification. *Phys. Rev. Lett.*, 102:173601, Apr 2009.

[27] J. Dressel, C. J. Broadbent, J. C. Howell, and A. N Jordan. Experimental violation of two-party leggett-garg inequalities with semiweak measurements. *Phys. Rev. Lett.*, 106(4):040402, 2011.

[28] Justin Dressel, Mehul Malik, Filippo M. Miatto, Andrew N. Jordan, and Robert W. Boyd. *Colloquium* : Understanding quantum weak values: Basics and applications. *Rev. Mod. Phys.*, 86:307–316, Mar 2014.

[29] Thomas Durt, Berthold-Georg Englert, Ingemar Bengtsson, and Karol Życzkowski. On mutually unbiased bases. *Int. J. Quantum Inf.*, 8(04):535–640, 2010.

[30] James S. Fakonas, Hyunseok Lee, Yousif A. Kelaita, and Harry A. Atwater. Two-plasmon quantum interference. *Nat. Photon.*, 8(4):317–320, Apr 2014.

[31] Joachim Fischbach and Matthias Freyberger. Quantum optical reconstruction scheme using weak values. *Phys. Rev. A*, 86(5):052110, 2012.

[32] N. Gisin and S. Massar. Optimal quantum cloning machines. *Phys. Rev. Lett.*, 79:2153–2156, Sep 1997.

[33] M. E. Goggin, M. P. Almeida, Marco Barbieri, B. P. Lanyon, J. L. O'Brien, A. G. White, and G. J. Pryde. Violation of the leggett–garg inequality with weak measurements of photons. *Proc. Natl. Acad. Sci.*, 108(4):1256–1261, 2011.

[34] Shay Hacohen-Gourgy, Leigh S. Martin, Emmanuel Flurin, Vinay V. Ramasesh, K. Birgitta Whaley, and Irfan Siddiqi. Quantum dynamics of simultaneously measured non-commuting observables. *Nature*, 538(7626):491–494, Oct 2016.

[35] MW Hamilton. Phase shifts in multilayer dielectric beam splitters. *Am. J. Phys.*, 68(2):186–191, 2000.

[36] Lucien Hardy. Quantum theory from five reasonable axioms. *arXiv:quant-ph/0101012*.

[37] W. Heisenberg. Über den anschaulichen inhalt der quantentheoretischen kinematik und mechanik. *Z. Phys.*, 43(3):172–198, 1927.

[38] Holger F. Hofmann. How weak values emerge in joint measurements on cloned quantum systems. *Phys. Rev. Lett.*, 109:020408, Jul 2012.

[39] C. K. Hong, Z. Y. Ou, and L. Mandel. Measurement of subpicosecond time intervals between two photons by interference. *Phys. Rev. Lett.*, 59:2044–2046, Nov 1987.

[40] Antonín Černoch, Jan Soubusta, Lucie Bartůšková, Miloslav Dušek, and Jaromír Fiurášek. Experimental realization of linear-optical partial swap gates. *Phys. Rev. Lett.*, 100:180501, May 2008.

[41] Asger C. Ipsen. Disturbance in weak measurements and the difference between quantum and classical weak values. *Phys. Rev. A*, 91:062120, Jun 2015.

[42] William T. M. Irvine, Antía Lamas Linares, Michiel J. A. de Dood, and Dirk Bouwmeester. Optimal quantum cloning on a beam splitter. *Phys. Rev. Lett.*, 92:047902, Jan 2004.

[43] A. N. Jordon. Viewpoint: Mapping out the state of a quantum system. *Physics*, 9(104), 2016.

[44] Richard Jozsa. Fidelity for mixed quantum states. *Journal of Modern Optics*, 41(12):2315–2323, 1994.

[45] Nadav Katz, Matthew Neeley, M. Ansmann, Radoslaw C. Bialczak, M. Hofheinz, Erik Lucero, A. O'Connell, H. Wang, A. N. Cleland, John M. Martinis, and Alexander N. Korotkov. Reversal of the weak measurement of a quantum state in a superconducting phase qubit. *Phys. Rev. Lett.*, 101:200401, Nov 2008.

[46] John G. Kirkwood. Quantum statistics of almost classical assemblies. *Phys. Rev.*, 44:31–37, Jul 1933.

[47] George C Knee, Joshua Combes, Christopher Ferrie, and Erik M Gauger. Weak-value amplification: state of play. *Quant. Meas. Quant. Metro.*, 3(1):32–37, 2016.

[48] Sacha Kocsis, Boris Braverman, Sylvain Ravets, Martin J Stevens, Richard P Mirin, L Krister Shalm, and Aephraim M Steinberg. Observing the average trajectories of single photons in a two-slit interferometer. *Science*, 332(6034):1170–1173, 2011.

[49] U. Leonhardt. *Measuring the Quantum State of Light*. Cambridge Studies in Modern Optics. Cambridge University Press, 1997.

[50] U. Leonhardt and H. Paul. Phase measurement and q function. *Phys. Rev. A*, 47:R2460–R2463, Apr 1993.

[51] R. Lopes, A. Imanaliev, A. Aspect, M. Cheneau, D. Boiron, and C. I. Westbrook. Atomic hong-ou-mandel experiment. *Nature*, 520(7545):66–68, Apr 2015.

[52] J. S. Lundeen and K. J. Resch. Practical measurement of joint weak values and their connection to the annihilation operator. *Phys. Lett. A*, 334(5):337–344, 2005.

[53] J. S. Lundeen and A. M. Steinberg. Experimental joint weak measurement on a photon pair as a probe of hardy's paradox. *Phys. Rev. Lett.*, 102(2):020404, 2009.

[54] Jeff S. Lundeen and Charles Bamber. Procedure for direct measurement of general quantum states using weak measurement. *Phys. Rev. Lett.*, 108:070402, Feb 2012.

[55] Jeff S. Lundeen, Brandon Sutherland, Aabid Patel, Corey Stewart, and Charles Bamber. Direct measurement of the quantum wavefunction. *Nature*, 474(7350):188–191, Jun 2011.

[56] A. I. Lvovsky and M. G. Raymer. Continuous-variable optical quantum-state tomography. *Rev. Mod. Phys.*, 81:299–332, Mar 2009.

[57] Jean-Philippe W. MacLean, Katja Ried, Robert W. Spekkens, and Kevin J. Resch. Quantum-coherent mixtures of causal relations. *Nat. Commun.*, 8:15149 EP –, May 2017.

[58] Mehul Malik, Mohammad Mirhosseini, Martin P. J. Lavery, Jonathan Leach, Miles J. Padgett, and Robert W. Boyd. Direct measurement of a 27-dimensional orbital-angular-momentum state vector. *Nat. Commun.*, 5:3115 EP –, Jan 2014. Article.

[59] Henry Margenau and Robert Nyden Hill. Correlation between measurements in quantum theory. *Progress of Theoretical Physics*, 26(5):722, 1961.

[60] Mohammad Mirhosseini, Omar S. Magaña Loaiza, Seyed Mohammad Hashemi Rafsanjani, and Robert W. Boyd. Compressive direct measurement of the quantum wave function. *Phys. Rev. Lett.*, 113:090402, Aug 2014.

[61] Graeme Mitchison. Weak measurement takes a simple form for cumulants. *Phys. Rev. A*, 77:052102, May 2008.

[62] José E Moyal. Quantum mechanics as a statistical theory. In *Mathematical Proceedings of the Cambridge Philosophical Society*, volume 45, pages 99–124. Cambridge University Press, 1949.

[63] Eleonora Nagali, Linda Sansoni, Fabio Sciarrino, Francesco De Martini, Lorenzo Marrucci, Bruno Piccirillo, Ebrahim Karimi, and Enrico Santamato. Optimal quantum cloning of orbital angular momentum photon qubits through hong-ou-mandel coalescence. *Nat. Photon.*, 3(12):720–723, Dec 2009.

[64] J. W. Noh, A. Fougères, and L. Mandel. Measurement of the quantum phase by photon counting. *Phys. Rev. Lett.*, 67:1426–1429, Sep 1991.

[65] Ognyan Oreshkov and Todd A. Brun. Weak measurements are universal. *Phys. Rev. Lett.*, 95:110409, Sep 2005.

[66] Masanao Ozawa. Universally valid reformulation of the heisenberg uncertainty principle on noise and disturbance in measurement. *Phys. Rev. A*, 67:042105, Apr 2003.

[67] Masanao Ozawa. Uncertainty relations for joint measurements of noncommuting observables. *Phys. Lett. A*, 320(5–6):367 – 374, 2004.

[68] Agustin Palacios-Laloy, François Mallet, François Nguyen, Patrice Bertet, Denis Vion, Daniel Esteve, and Alexander N Korotkov. Experimental violation of a bell/'s inequality in time with weak measurement. *Nat. Phys.*, 6(6):442–447, 2010.

[69] James L. Park and Henry Margenau. Simultaneous measurability in quantum theory. *International Journal of Theoretical Physics*, 1(3):211–283, 1968.

[70] Raj B. Patel, Joseph Ho, Franck Ferreyrol, Timothy C. Ralph, and Geoff J. Pryde. A quantum fredkin gate. *Science Adv.*, 2(3), 2016.

[71] Wolfgang Pauli. *Theory of Measurements*, pages 67–78. Springer Berlin Heidelberg, Berlin, Heidelberg, 1980.

[72] F. Piacentini, A. Avella, M. P. Levi, M. Gramegna, G. Brida, I. P. Degiovanni, E. Cohen, R. Lussana, F. Villa, A. Tosi, F. Zappa, and M. Genovese. Measuring incompatible observables by exploiting sequential weak values. *Phys. Rev. Lett.*, 117:170402, Oct 2016.

[73] F. Piacentini, A. Avella, M. P. Levi, R. Lussana, F. Villa, A. Tosi, F. Zappa, M. Gramegna, G. Brida, I. P. Degiovanni, and M. Genovese. Experiment investigating the connection between weak values and contextuality. *Phys. Rev. Lett.*, 116:180401, May 2016.

[74] Gilles Putz, Tomer Barnea, Nicolas Gisin, and Anthony Martin. Experimental weak measurement of two non-commuting observables. *arXiv:quant-ph/1610.04464*.

[75] M. G. Raymer. Measuring the quantum mechanical wave function. *Contemp. Phys.*, 38(5):343–355, 1997.

[76] Joseph M. Renes, Robin Blume-Kohout, A. J. Scott, and Carlton M. Caves. Symmetric informationally complete quantum measurements. *J. Math. Phys.*, 45(6):2171–2180, 2004.

[77] Kevin J Resch, Jeff S Lundeen, and Aephraim M Steinberg. Experimental realization of the quantum box problem. *Phys. Lett. A*, 324(2):125–131, 2004.

[78] Martin Ringbauer, Devon N. Biggerstaff, Matthew A. Broome, Alessandro Fedrizzi, Cyril Branciard, and Andrew G. White. Experimental joint quantum measurements with minimum uncertainty. *Phys. Rev. Lett.*, 112:020401, Jan 2014.

[79] N. W. M. Ritchie, J. G. Story, and Randall G. Hulet. Realization of a measurement of a "weak value". *Phys. Rev. Lett.*, 66:1107–1110, Mar 1991.

[80] H. P. Robertson. The uncertainty principle. *Phys. Rev.*, 34:163–164, Jul 1929.

[81] Lee A. Rozema, Ardavan Darabi, Dylan H. Mahler, Alex Hayat, Yasaman Soudagar, and Aephraim M. Steinberg. Violation of heisenberg's measurement-disturbance relationship by weak measurements. *Phys. Rev. Lett.*, 109:100404, Sep 2012.

[82] Jeff Z. Salvail, Megan Agnew, Allan S. Johnson, Eliot Bolduc, Jonathan Leach, and Robert W. Boyd. Full characterization of polarization states of light via direct measurement. *Nat. Photon.*, 7(4):316–321, Apr 2013.

[83] Valerio Scarani, Sofyan Iblisdir, Nicolas Gisin, and Antonio Acín. Quantum cloning. *Rev. Mod. Phys.*, 77:1225–1256, Nov 2005.

[84] J. Shapiro and S. Wagner. Phase and amplitude uncertainties in heterodyne detection. *IEEE J. Quant. Electron.*, 20(7):803–813, Jul 1984.

[85] C. Y. She and H. Heffner. Simultaneous measurement of noncommuting observables. *Phys. Rev.*, 152:1103–1110, Dec 1966.

[86] Zhimin Shi, Mohammad Mirhosseini, Jessica Margiewicz, Mehul Malik, Freida Rivera, Ziyi Zhu, and Robert W. Boyd. Scan-free direct measurement of an extremely high-dimensional photonic state. *Optica*, 2(4):388–392, Apr 2015.

[87] Itay Shomroni, Orel Bechler, Serge Rosenblum, and Barak Dayan. Demonstration of weak measurement based on atomic spontaneous emission. *Phys. Rev. Lett.*, 111:023604, Jul 2013.

[88] Christoph Simon, Gregor Weihs, and Anton Zeilinger. Optimal quantum cloning via stimulated emission. *Phys. Rev. Lett.*, 84(13):2993, 2000.

[89] D. T. Smithey, M. Beck, M. G. Raymer, and A. Faridani. Measurement of the wigner distribution and the density matrix of a light mode using optical homodyne tomography: Application to squeezed states and the vacuum. *Phys. Rev. Lett.*, 70:1244–1247, Mar 1993.

[90] Aephraim M. Steinberg. Conditional probabilities in quantum theory and the tunneling-time controversy. *Phys. Rev. A*, 52:32–42, Jul 1995.

[91] Aephraim M Steinberg. How much time does a tunneling particle spend in the barrier region? *Phys. Rev. Lett.*, 74(13):2405, 1995.

[92] Yutaro Suzuki, Masataka Iinuma, and Holger F Hofmann. Observation of non-classical correlations in sequential measurements of photon polarization. *New J. Phys.*, 18(10):103045, 2016.

[93] G. S. Thekkadath, L. Giner, Y. Chalich, M. J. Horton, J. Banker, and J. S. Lundeen. Direct measurement of the density matrix of a quantum system. *Phys. Rev. Lett.*, 117:120401, Sep 2016.

[94] Giuseppe Vallone and Daniele Dequal. Strong measurements give a better direct measurement of the quantum wave function. *Phys. Rev. Lett.*, 116:040502, Jan 2016.

[95] J. Von Neumann. *Mathematical Foundations of Quantum Mechanics*. Investigations in physics. Princeton University Press, 1955.

[96] E. Wigner. On the quantum correction for thermodynamic equilibrium. *Phys. Rev.*, 40:749–759, Jun 1932.

[97] H. M. Wiseman. Weak values, quantum trajectories, and the cavity-qed experiment on wave-particle correlation. *Phys. Rev. A*, 65:032111, Feb 2002.

[98] W. K. Wootters and W. H. Zurek. A single quantum cannot be cloned. *Nature*, 299(5886):802–803, Oct 1982.

[99] William K Wootters and Brian D Fields. Optimal state-determination by mutually unbiased measurements. *Ann. Phys.*, 191(2):363 – 381, 1989.

[100] Shengjun Wu. State tomography via weak measurements. *Sci. Rep.*, 3, 2013.

[101] Kazuhiro Yokota, Takashi Yamamoto, Masato Koashi, and Nobuyuki Imoto. Direct observation of hardy's paradox by joint weak measurement with an entangled photon pair. *New J. Phys.*, 11(3):033011, 2009.

[102] Nicole Yunger Halpern. Jarzynski-like equality for the out-of-time-ordered correlator. *Phys. Rev. A*, 95:012120, Jan 2017.

Appendix A

Density matrix and mixed states

In this thesis, we have seen that there are numerous ways of describing the state of quantum systems. The most notorious object, the wave function, is in fact quite limited. It cannot describe what are known as *mixed states*, which are statistical mixtures of pure states. To describe these, one requires either a quasiprobability distribution such as the Wigner or Dirac distributions, or the density matrix.

The density matrix is defined in the following way:

$$\boldsymbol{\rho} = \sum_i p_i \left|\psi_i\right\rangle \left\langle\psi_i\right| \tag{A.1}$$

where p_i is the probability of the system being in a particular pure state $|\psi_i\rangle$. A physical density matrix must satisfy the following properties:

1. Hermitian: $\boldsymbol{\rho}^\dagger = \boldsymbol{\rho}$
2. Positive semi-definite: $\boldsymbol{\rho} \geq 0$, *i.e.* its eigenvalues are non-negative
3. Normalized: $\mathrm{Tr}(\boldsymbol{\rho}) = 1$

The density matrix can also be used to describe pure states, in which case, $\boldsymbol{\rho} = \boldsymbol{\rho}^2$. In general, $\mathrm{Tr}(\boldsymbol{\rho}^2)$ is a quantity known as the *purity* and quantifies the degree of mixedness of the state. For a d-dimensional state, the purity is a number that lies between 1 (pure) and $1/d$ (completely mixed). As is the case with quasiprobability distributions, quantum mechanics can be completely reformulated in terms of density matrices. For example, the expectation value of an operator $\boldsymbol{A}$ is computed using:

$$\langle \boldsymbol{A} \rangle = \mathrm{Tr}(\boldsymbol{A}\boldsymbol{\rho}) = \sum_i p_i \left\langle\psi_i\right| A \left|\psi_i\right\rangle \tag{A.2}$$

But why do we need to consider mixed states at all? A classic example to draw the distinction between pure and mixed states is the following. Suppose a photon is diagonally polarized, which is an equal superposition of being horizontally and vertically polarized: $|\psi\rangle = (|H\rangle + |V\rangle)/\sqrt{2}$. In this case, the density matrix (expressed in the H/V basis) is:

$$\boldsymbol{\rho} = |\psi\rangle\langle\psi| = \begin{pmatrix} \langle H|\boldsymbol{\rho}|H\rangle & \langle H|\boldsymbol{\rho}|V\rangle \\ \langle V|\boldsymbol{\rho}|H\rangle & \langle V|\boldsymbol{\rho}|V\rangle \end{pmatrix} = \frac{1}{2}\begin{pmatrix} 1 & 1 \\ 1 & 1 \end{pmatrix} \tag{A.3}$$

One can check that $\boldsymbol{\rho} = \boldsymbol{\rho}^2$, and so this is a pure state. The diagonals are the probabilities for the state to be either $|H\rangle$ or $|V\rangle$. The off-diagonals are known as *coherences*, and their physical significance is a little more subtle. To understand their role, suppose that we made them zero, such that

$$\boldsymbol{\rho} = \frac{1}{2}(|H\rangle\langle H| + |V\rangle\langle V|) = \frac{1}{2}\begin{pmatrix} 1 & 0 \\ 0 & 1 \end{pmatrix}. \tag{A.4}$$

One can check that the purity of this state, $\mathrm{Tr}(\boldsymbol{\rho}^2)$, is minimal. Indeed, this state describes a photon which is in a statistical mixture: it has an equal probability of being horizontally polarized and vertically polarized. Of course, the diagonally polarized photon shares the same feature. However, there is a physical difference between these two photons. This difference can be detected using a polarizer. By aligning the polarizer along the diagonal, the diagonally polarized photons will transmit without attenuation, whereas the statistical mixture will be attenuated by half. Thus, the coherences tell us something about whether the photon is *simultaneously* $|H\rangle$ and $|V\rangle$ (superposition), or *sometimes* $|H\rangle$ and/or $|V\rangle$. In less hand-waving words, the coherences quantify correlations in the phase of an electromagnetic field along its horizontal and vertical axes. For this reason, coherences are a basis-dependent quantity. For example, while $\boldsymbol{\rho} = |H\rangle\langle H|$ has no coherences, it can be re-written in the diagonal/anti-diagonal basis to have coherences:

$$\boldsymbol{\rho} = |H\rangle\langle H| = \frac{1}{2}(|D\rangle + |A\rangle)(\langle D| + \langle A|) = \frac{1}{2}\begin{pmatrix} 1 & 1 \\ 1 & 1 \end{pmatrix}. \tag{A.5}$$

Mixed states can be generated by introducing noise in an experiment, as was done in the density matrix experiment of Ch. 3. They also arise naturally in multipartite systems. Consider a two-particle system $\boldsymbol{H} = \boldsymbol{H}_A \otimes \boldsymbol{H}_B$. The fact that we combine two Hilbert spaces gives rise to new states that do not exist locally in each sub-space, *i.e.* $|\Psi\rangle \in \boldsymbol{H}$, but $|\Psi\rangle \neq |\psi_1\rangle_A \otimes |\psi_2\rangle_B$ where $|\psi_1\rangle_A \in$

$\boldsymbol{H}_A$ and $|\psi_2\rangle_B \in \boldsymbol{H}_B$. States like $|\Psi\rangle$ are *entangled*. If a state is entangled, then its subsystems are mixed states. The degree of mixedness of the subsystems depends directly on the degree of entanglement of $|\Psi\rangle$.

Appendix B

Fidelity and trace distance

Experiments are never perfect. These imperfections can be estimated by comparing the output of the experiment to what is expected theoretically. In particular, in both experiments of Ch. 3 and Ch. 5, we would like to know how similar our measured states are to the ideal state. Such a metric also plays a key role in many analytical problems in quantum information, such as proving optimal cloning (see Ch. 4).

In the case of pure states, it is easy to quantify how similar two states are. In matrix mechanics, the inner product gives the overlap between two vectors representing the states:

$$\left|\langle\psi|\phi\rangle\right|^2. \tag{B.1}$$

In the case of wave mechanics, one can compute the overlap integral between two wave functions:

$$\int_{\infty}^{\infty} dx\psi^*(x)\phi(x) \tag{B.2}$$

Indeed, Eq. B.1 and Eq. B.2 are in fact the same. In the context of atomic physics, these equations give the probability for *e.g.* an electron to transition from one state $|\psi\rangle$ to another $|\phi\rangle$, hence the name *transition probability*.

Similarly, we want to extend this idea and find a metric that quantifies the similarity between two mixed quantum states represented by the density matrices $\boldsymbol{\rho}$ and $\boldsymbol{\beta}$. The difference is of course that mixed states are statistical mixtures of pure states. It turns out that there are many such metrics for density matrices. This is not surprising, since there is also no single way to determine the distance between two classical probability distributions.

Probably the most popular metric is the *fidelity* $F(\boldsymbol{\rho},\boldsymbol{\beta})$, developed by Canadian physicist R. Jozsa in 1994 [44]. It is based on the following desired proper-

ties:

1. $0 \leq F(\boldsymbol{\rho}, \boldsymbol{\beta}) \leq 1$, and $F(\boldsymbol{\rho}, \boldsymbol{\beta}) = 1$ if and only if $\boldsymbol{\rho} = \boldsymbol{\beta}$
2. $F(\boldsymbol{\rho}, \boldsymbol{\beta}) = F(\boldsymbol{\beta}, \boldsymbol{\rho})$
3. If $\boldsymbol{\rho} = |\psi\rangle\langle\psi|$ and $\boldsymbol{\beta} = |\phi\rangle\langle\phi|$ are pure, then $F(\boldsymbol{\rho}, \boldsymbol{\beta}) = \left|\langle\psi|\beta\rangle\right|^2$
4. $F(\boldsymbol{\rho}, \boldsymbol{\beta})$ is invariant under unitary transformation

In other words, Jozsa was looking for a metric similar to the transition probability of pure states. He found that a formula satisfying all of these properties is:

$$F(\boldsymbol{\rho}, \boldsymbol{\beta}) = \mathrm{Tr}\left(\sqrt{\sqrt{\boldsymbol{\rho}}\boldsymbol{\beta}\sqrt{\boldsymbol{\rho}}}\right)^2. \tag{B.3}$$

Note that some people use the fidelity without the square outside the trace. I think it is important to keep since it gives the fidelity the meaning of being a probability. For example, a fidelity of $F(\boldsymbol{\rho}, \boldsymbol{\beta}) = 0.99$ means that there is a 99% chance that the states are $\boldsymbol{\rho}$ and $\boldsymbol{\beta}$ are the same.

Another useful metric is the *trace distance*:

$$T(\boldsymbol{\rho}, \boldsymbol{\beta}) = \frac{1}{2}\mathrm{Tr}\sqrt{(\boldsymbol{\rho} - \boldsymbol{\beta})(\boldsymbol{\rho} - \boldsymbol{\beta})^\dagger} \tag{B.4}$$

In contrast to the fidelity, the formula for the trace distance does not assume that the density matrices are Hermitian nor positive semi-definite. Although these are required for a physical state, experimental error in Ch. 3 sometimes meant that our matrices were neither. However, if the density matrices are physical, then the trace distance has two nice physical interpretations. In the case of qubits, as in Ch. 3, it is half the Euclidean distance between the states on the Bloch sphere. More generally, it is a measure of the maximum probability of distinguishing between $\boldsymbol{\rho}$ and $\boldsymbol{\beta}$, with an optimal measurement. The relation between the fidelity and the trace distance is given by the following equation:

$$1 - F(\boldsymbol{\rho}, \boldsymbol{\beta}) \leq T(\boldsymbol{\rho}, \boldsymbol{\beta}) \leq \sqrt{1 - F(\boldsymbol{\rho}, \boldsymbol{\beta})}. \tag{B.5}$$

Appendix C

Input-output relations of a beam splitter

The beam splitter (BS) is an optical device that reflects and transmits light. We often learn in our undergraduate studies that light being reflected from a surface gives rise to a phase shift of $\pi/2$. In fact, this is not always true. Here, we derive a generalized condition for the phase acquired by the light as it reflects and transmits at a BS. The derivation is done in second quantization and impinges on the fact that the commutator relation of the electromagnetic field must be conserved before and after the BS. However, a similar derivation can also be achieved with classical fields, where the same result is obtained from energy conservation.

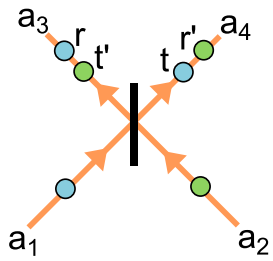

Figure C.1: The beam splitter.

A beam splitter is shown in Fig. C.1. In terms of input modes, the output of the BS is

$$\boldsymbol{a}_3 = r\,\boldsymbol{a}_1 + t'\,\boldsymbol{a}_2 \quad \text{and} \quad \boldsymbol{a}_4 = t\,\boldsymbol{a}_1 + r'\,\boldsymbol{a}_2 \tag{C.1}$$

where r and r' are complex probability amplitudes for reflection, and t and t' are complex probability amplitudes for transmission. We want to determine conditions on the phase relation betweens these coefficients.

A property which must remain constant before and after BS is the commutation relation between the fields in each mode. Namely,

$$[\boldsymbol{a}_i, \boldsymbol{a}_j^\dagger] = \delta_{ij} \quad \text{and} \quad [\boldsymbol{a}_i, \boldsymbol{a}_j] = 0 = [\boldsymbol{a}_i^\dagger, \boldsymbol{a}_j^\dagger] \tag{C.2}$$

Expanding these using Eq. C.1, one finds that these commutation relations are satisfied if and only if:

$$|r'| = |r| \ , \ |t| = |t'| \ , \ |r|^2 + |t|^2 = 1 \ , \ r^* t' + r' t^* = 0 \ , \ r^* t + r' t'^* = 0. \tag{C.3}$$

These equations fix the phase relations between all the input and output fields.

Consider a 50:50 BS, which ideally, evenly splits the light, meaning $|r|^2 = |r'|^2 = |t|^2 = |t'|^2 = 1/2$. This type of BS is typically constructed to have a single reflection surface (interface between two cemented glass prisms), which leads to the well known phase shift of $\pi/2$. Indeed, setting $r = r' = \exp(i\pi/2)/\sqrt{2} = i/\sqrt{2}$ and $t = t' = 1/\sqrt{2}$ is one of the possible ways to satisfy Eq. C.3. In that case,

$$\boldsymbol{a}_3 = (i\,\boldsymbol{a}_1 + \boldsymbol{a}_2)/\sqrt{2} \quad \text{and} \quad \boldsymbol{a}_4 = (\boldsymbol{a}_1 + i\,\boldsymbol{a}_2)/\sqrt{2} \tag{C.4}$$

In general, the phases of r and t will depend on the construction of the optical device [35].